Supporting Information:

An Efficient Integrator Scheme for Sampling the (Quantum) Isobaric-Isothermal Ensemble in (Path Integral) Molecular Dynamics Simulations

Weihao Liang[1,†], Sihan Wang[1,†], Cong Wang[1,2,†], Weizhou Wang[1], Xinchen She[1], Chongbin Wang[1], Jiushu Shao[2], Jian Liu[1,]*

1. Beijing National Laboratory for Molecular Sciences, Institute of Theoretical and Computational Chemistry, College of Chemistry and Molecular Engineering, Peking University, Beijing 100871, China
2. College of Chemistry and Center for Advanced Quantum Studies, Key Laboratory of Theoretical and Computational Photochemistry, Ministry of Education, Beijing Normal University, Beijing, 100875, China

(Invited Contribution to *Journal of Chemical Theory and Computation*)

AUTHOR INFORMATION

Corresponding Author

* Electronic mail: jianliupku@pku.edu.cn

Author Contributions

† W. Liang, S. Wang, and C. Wang contributed equally.

S1. Evaluation of Thermodynamic Properties in MD and PIMD Simulations

S1-A: PIMD Simulations of the NPT Ensemble

Path integral molecular dynamics (PIMD) is an efficient tool for sampling statistical properties that involve nuclear quantum effects, such as tunneling and zero-point energy. These effects are particularly important in systems containing light atoms or those at low temperatures. In PIMD, each atom is mapped onto a classical ring polymer, where the "beads" are connected by harmonic springs. When isotropic systems are studied, a scalar pressure is required to evolve the volume of the system. To derive the internal scalar pressure in PIMD, we begin with the partition function under the path integral formulation of the canonical ensemble

$$\begin{aligned} Z_{\mathrm{NVT}} &= \mathrm{Tr}\left[\exp\left(-\beta\hat{H}\right)\right] = \int_{D(V)} \mathrm{d}\mathbf{x}\langle\mathbf{x}\,|\,\exp(-\beta\hat{H})\,|\,\mathbf{x}\rangle \\ &\equiv I_{\mathrm{PI}} \lim_{L\to\infty} \int_{D(V)} \mathrm{d}\mathbf{x}_1 \int_{D(V)} \mathrm{d}\mathbf{x}_2 \cdots \int_{D(V)} \mathrm{d}\mathbf{x}_L \exp\left[-\beta U_{\mathrm{eff}}(\mathbf{x}_1,\cdots,\mathbf{x}_L)\right], \end{aligned} \tag{S1}$$

where $U_{\mathrm{eff}}\left(\mathbf{x}_1,\cdots,\mathbf{x}_L\right) = \sum_{i=1}^{L} \frac{1}{2}\omega_L^{\,2}\left[\left(\mathbf{x}_{i+1}-\mathbf{x}_i\right)^T \mathbf{M}\left(\mathbf{x}_{i+1}-\mathbf{x}_i\right)\right] + \frac{1}{L}\sum_{i=1}^{L} U\left(\mathbf{x}_i\right)$ is the effective potential of the path integral beads, L is the number of beads, $I_{\mathrm{PI}} = \left(L/2\pi\beta\hbar^2\right)^{3NL/2}\left|\mathbf{M}\right|^{L/2}$ is a normalization factor, and $\omega_L = \frac{\sqrt{L}}{\beta\hbar}$ is the frequency of the springs between beads. Thermodynamic properties are of the general form

$$\begin{aligned} \langle\hat{B}\rangle_{\mathrm{NVT}}^{\mathrm{QM}} &= \frac{1}{Z_{\mathrm{NVT}}}\mathrm{Tr}\left[\exp\left(-\beta\hat{H}\right)\hat{B}\right] = \\ &\frac{1}{Z_{\mathrm{NVT}}} I_{\mathrm{PI}} \lim_{L\to\infty} \prod_{j=1}^{L}\left(\int_{D(V)} \mathrm{d}\mathbf{x}_j\right)\exp\left[-\beta U_{\mathrm{eff}}(\mathbf{x}_1,\cdots,\mathbf{x}_L)\right]\tilde{B}(\mathbf{x}_1,\cdots,\mathbf{x}_L), \end{aligned} \tag{S2}$$

where $\hat{B}$ represents the quantum mechanical operator. The estimator $\tilde{B}(\mathbf{x}_1,\cdots,\mathbf{x}_L)$ for any coordinate dependent operator is given by

$$\tilde{B}(\mathbf{x}_1,\cdots,\mathbf{x}_L)=\frac{1}{L}\sum_{i=1}^{L}B(\mathbf{x}_i). \tag{S3}$$

For kinetic energy operator $\hat{B}=\frac{1}{2}\hat{\mathbf{p}}^T\mathbf{M}^{-1}\hat{\mathbf{p}}$, the primitive form ($K_{\text{prim}}^{\text{QM}}$)is

$$\tilde{B}(\mathbf{x}_1,\cdots,\mathbf{x}_L)=K_{\text{prim}}^{\text{QM}}=\frac{N_f L}{2\beta}-\sum_{i=1}^{L}\frac{1}{2}\omega_L^2\left[\left(\mathbf{x}_{i+1}-\mathbf{x}_i\right)^T\mathbf{M}\left(\mathbf{x}_{i+1}-\mathbf{x}_i\right)\right], \tag{S4}$$

and the virial form $K_{\text{vir}}^{\text{QM}}$ is[1]

$$\tilde{B}(\mathbf{x}_1,\cdots,\mathbf{x}_L)=K_{\text{vir}}^{\text{QM}}=\frac{N_f}{2\beta}+\frac{1}{2L}\sum_{i=1}^{L}\left[\left(\mathbf{x}_i-\mathbf{x}^*\right)^T\frac{\partial U(\mathbf{x}_i)}{\partial\mathbf{x}_i}\right], \tag{S5}$$

$\mathbf{x}^*$ can be the centroid of the ring polymer $\mathbf{x}^*=\frac{1}{L}\sum_{i=1}^{L}\mathbf{x}_i$, or any individual bead of the ring polymer $\mathbf{x}^*=\mathbf{x}_i$.

Similar to the classical case, the partition function for the isobaric-isothermal ensemble is expressed as[2]

$$Z_{\text{NPT}}=\frac{I_{\text{PI}}}{V_0}\int_0^\infty \mathrm{d}V\exp[-\beta PV]Z_{\text{NVT}}. \tag{S6}$$

Hence, thermodynamic properties of the isobaric-isothermal ensemble are given by

$$\begin{aligned}\langle\hat{B}\rangle_{\text{NPT}}^{\text{QM}}&=\frac{1}{V_0 Z_{\text{NPT}}}\int_0^\infty \mathrm{d}V\exp\left[-\beta PV\right]\mathrm{Tr}\left[e^{-\beta\hat{H}}\hat{B}\right]\\&=\frac{1}{V_0 Z_{\text{NPT}}}I_{\text{PI}}\lim_{L\to\infty}\int_0^\infty \mathrm{d}V\prod_{j=1}^{L}\left(\int_{D(V)}\mathrm{d}\mathbf{x}_j\right)e^{-\beta\left[PV+U_{\text{eff}}(\mathbf{x}_1,\cdots,\mathbf{x}_L)\right]}\tilde{B}(\mathbf{x}_1,\cdots,\mathbf{x}_L,V).\end{aligned} \tag{S7}$$

The staging transformation is used in this paper, in which the transformation of coordinates and forces is defined as[3, 4]

$$
\begin{aligned}
&\xi_1 = \mathbf{x}_1, \\
&\xi_i = \mathbf{x}_i - \frac{(i-1)\mathbf{x}_{i+1} + \mathbf{x}_1}{i} \quad (i = 2, \cdots, L), \\
&\frac{\partial \phi}{\partial \xi_1} = \frac{1}{L}\sum_{i=1}^{L} U'(\mathbf{x}_i), \\
&\frac{\partial \phi}{\partial \xi_i} = \frac{\partial \phi}{\partial \mathbf{x}_i} + \frac{i-2}{i-1}\frac{\partial \phi}{\partial \xi_{i-1}} \qquad (i = 2, \cdots, L),
\end{aligned}
\tag{S8}
$$

where ϕ is defined as $\phi(\xi_1, \cdots, \xi_L) = \frac{1}{L}\sum_{i=1}^{L} U\left[\mathbf{x}_i\left(\xi_1, \cdots, \xi_L\right)\right]$. The effective potential after staging transformation can be expressed as

$$
U_{\text{eff}}(\xi_1, \cdots, \xi_L) = \sum_{i=1}^{L} \frac{1}{2}\omega_L^2 \xi_i^T \overline{\mathbf{M}} \xi_i + \frac{1}{L}\sum_{i=1}^{L} U\left[\mathbf{x}_i(\xi_1, \cdots, \xi_L)\right]. \tag{S9}
$$

The corresponding mass matrix of the staging transformation is given by

$$
\begin{aligned}
&\overline{\mathbf{M}}_1 = 0, \\
&\overline{\mathbf{M}}_i = \frac{i}{i-1}\mathbf{M} \qquad (i = 2, \cdots, L).
\end{aligned}
\tag{S10}
$$

To apply MD in the path integral presentation, fictitious momenta $(\mathbf{p}_1, \cdots, \mathbf{p}_L)$ are introduced to the beads of the ring polymer, which produces the PIMD approach. The effective Hamiltonian can be given by

$$
H_{\text{eff}}(\mathbf{x}_1, \cdots, \mathbf{x}_L, \mathbf{p}_1, \cdots, \mathbf{p}_L) = \sum_{i=1}^{L} \frac{1}{2}\mathbf{p}_i^T \mathbf{M}_i^{-1} \mathbf{p}_i + U_{\text{eff}}(\mathbf{x}_1, \cdots, \mathbf{x}_L). \tag{S11}
$$

where $\mathbf{M}$ is the fictitious mass,

$$
\begin{aligned}
&\mathbf{M}_1 = \mathbf{M}, \\
&\mathbf{M}_i = \frac{i}{i-1}\mathbf{M} \qquad (i = 2, \cdots, L).
\end{aligned}
\tag{S12}
$$

S1-B. Estimation of the Internal Pressure, and Difference between the "All-mode Scaled" Method and "Reduced Dynamics" Method for the MTTK Barostat in PIMD

From eq (S11), the internal pressure in the path integral formation is expressed as an analogy to the classical form by using the effective potential

$$P_{\text{int}}^{\text{PI,all-mode}} = \frac{1}{dV}\sum_{i=1}^{L}\left(\mathbf{p}_i^T\mathbf{M}_i^{-1}\mathbf{p}_i - \omega_L^2\boldsymbol{\xi}_i^T\overline{\mathbf{M}}_i\boldsymbol{\xi}_i - \left(\frac{\partial\phi}{\partial\boldsymbol{\xi}_i}\right)^T\boldsymbol{\xi}_i\right). \tag{S13}$$

In comparison, the virial expression of the internal pressure in classical statistical mechanics is

$$P_{\text{int}}^{\text{CM}} = \frac{1}{dV}\left(\mathbf{p}^T\mathbf{M}^{-1}\mathbf{p} - \mathbf{x}^T\frac{\partial U}{\partial\mathbf{x}}\right). \tag{S14}$$

When PIMD uses eq (S13) as the virial expression of the internal pressure, it is often referred to as the "all-mode scaled" method.

In classical MD, the molecular virial is often used instead of the atomic virial to estimate the internal pressure due to the scale separation between intra- and intermolecular interactions. Details of the molecular virial are shown in Section S4. Martyna *et al.* proposed it for the PIMD simulation[2], because the frequency of the harmonic spring between beads is higher than the typical frequencies of molecules. Thus, the isomorphic ring polymer can be treated as a "quasi-molecule", with the harmonic potential between beads as the intramolecular potential. This approach is referred to as the "reduced dynamics" method. In this case, the internal pressure takes the form:

$$P_{\text{int}}^{\text{PI,reduced}} = \frac{1}{dV}\left(\mathbf{p}_1^T\mathbf{M}_1^{-1}\mathbf{p}_1 - \boldsymbol{\xi}_1^T\frac{\partial\phi}{\partial\boldsymbol{\xi}_1}\right), \tag{S15}$$

where $\boldsymbol{\xi}_1, \mathbf{p}_1, \mathbf{M}_1$ represents the coordinate, momentum and mass matrix of the first staging mode. The rescaling of the coordinate and momentum in the equations of motion, corresponding to phase

space evolution operators $e^{\mathcal{L}_{x_t}\Delta t}$ and $e^{\mathcal{L}_{p_t}\Delta t}$ in the "reduced dynamics" method, is then different from that of the "all-mode scaled" method. In the "all-mode scaled" method, the coordinate and momentum variables of all path integral beads are rescaled. As comparison, in the "reduced dynamics" method, only the coordinate and momentum of the first staging mode are rescaled. The corresponding equations of motion are:

$$\begin{cases} \dot{\boldsymbol{\xi}}_i = \dfrac{p_\varepsilon}{W}\boldsymbol{\xi}_i \\ \dot{\mathbf{p}}_i = \left(1+\dfrac{d}{N_f L}\right)\dfrac{p_\varepsilon}{W}\mathbf{p}_i \end{cases} \quad (i=1,\cdots,L), \tag{S16}$$

for the "all-mode scaled" method, and

$$\begin{cases} \dot{\boldsymbol{\xi}}_1 = \dfrac{p_\varepsilon}{W}\boldsymbol{\xi}_1 \\ \dot{\mathbf{p}}_1 = \left(1+\dfrac{d}{N_f}\right)\dfrac{p_\varepsilon}{W}\mathbf{p}_1 \end{cases}. \tag{S17}$$

for the "reduced dynamics" method.

The internal pressure expression of the "all-mode scaled" method and that of the "reduced dynamics" method can be demonstrated to be equivalent through the virial theorem

$$\frac{N_f(L-1)}{\beta} - \left\langle \sum_{i=1}^{L} \omega_L^2 \boldsymbol{\xi}_i^T \overline{\mathbf{M}}_i \boldsymbol{\xi}_i \right\rangle = \frac{1}{L}\left\langle \left(\frac{\partial U(\mathbf{x}_i)}{\partial \mathbf{x}_i}\right)^T (\mathbf{x}_i - \mathbf{x}_1) \right\rangle, \tag{S18}$$

By substituting eq (S18) and the staging transformation formula eq (S8) into eq (S13), we obtain:

$$P_{\text{int}}^{\text{PI,reduced}} = \frac{1}{dV}\left[\mathbf{p}_1^T \mathbf{M}_1^{-1} \mathbf{p}_1 + \frac{1}{L}\sum_{i=1}^{L}\left(\frac{\partial U(\mathbf{x}_i)}{\partial \mathbf{x}_i}\right)^T (\mathbf{x}_i - \mathbf{x}_1) - \frac{1}{L}\sum_{i=1}^{L}\left(\frac{\partial U(\mathbf{x}_i)}{\partial \mathbf{x}_i}\right)^T \mathbf{x}_i \right]. \tag{S19}$$

Eq (S19) can be obtained directly by subtracting the latter two terms without periodic boundary conditions. When periodic boundary conditions are employed, the corresponding conditions become more complex, but eq (S19) remains valid. In this paper, we use eq (S19) to estimate the

internal pressure of the "reduced dynamics".

In MD/PIMD simulations, we often apply the cutoff for short-range interactions. It is essential to incorporate corrections to account for the contributions of particles beyond the cutoff to both the potential energy and pressure. For the pairwise interaction $u(r)$, the total potential energy per particle can be expressed as

$$\frac{U}{N} = 2\pi\rho_{\text{ins}} \int \mathrm{d}r\, u(r) g(r) r^2, \tag{S20}$$

where $g(r)$ is the radial distribution function (RDF). Similarly, the pressure in classical statistical mechanics can be expressed as

$$P_{\text{int}}^{\text{CM}} = \rho k_B T - \frac{2\pi\rho^2}{3} \int \mathrm{d}r\, u'(r) g(r)\, r^3 \quad . \tag{S21}$$

In eq (S20) and eq (S21) the instantaneous density $\rho_{\text{ins}} = N/V$ is used.

Employ the Lennard-Jones (L-J) potential $u(r) = 4\varepsilon\left[\left(\frac{\sigma}{r}\right)^{12} - \left(\frac{\sigma}{r}\right)^{6}\right]$ as an example[2]. When a soft cutoff is applied to the L-J potential, it is defined by

$$\begin{aligned} &\tilde{u}(r) = u(r) S(r), \\ &S(r) = \begin{cases} 1 & r < r_c - \lambda, \\ 1 + \tilde{r}^2 (2\tilde{r} - 3) & r_c - \lambda \le r \le r_c, \\ 0 & r > r_c, \end{cases} \quad , \\ &\tilde{r} = \frac{r - r_c}{\lambda} + 1. \end{aligned} \tag{S22}$$

where r_c is the cutoff distance, and λ is the healing length for the soft cutoff. We assume that $g(r) \approx 1$ for $r > r_c - \lambda$. Substituting eq (S22) into eq (S20) as well as into eq (S21), we obtain the correction terms

$$\begin{aligned}\frac{\Delta U_{\text{corr}}^{\text{L-J,soft}}}{N} &= 2\pi\rho\int \mathrm{d}r\, u(r)\big(1-S(r)\big)\, g(r) r^2 \\ &= 2\pi\rho\left[\int_{r_c-\lambda}^{r_c} \mathrm{d}r\, u(r) r^2 \tilde{r}^2 (3-2\tilde{r}) + \int_{r_c}^{\infty} \mathrm{d}r\, u(r) r^2\right]\end{aligned} \tag{S23}$$

$$\Delta P_{\text{corr}}^{\text{L-J,soft}} = -\frac{2\pi\rho^2}{3}\int \mathrm{d}r \frac{\mathrm{d}\big(u(r)S(r)\big)}{\mathrm{d}r} g(r) r^3. \tag{S24}$$

By neglecting the r^{-12} term in the Lennard-Jones (L-J) potential and assuming $g(r)=1$ beyond the cutoff distance, the correction to the potential energy per particle and that to the pressure can be derived from eq (S23) and eq (S24)

$$\frac{\Delta U_{\text{corr}}^{\text{L-J,soft}}}{N} = -\frac{8\pi\varepsilon\sigma^6\rho}{\lambda^3}\left(\frac{1}{s_c}+\frac{1}{s_c-1}+2\ln\frac{s_c-1}{s_c}\right), \tag{S25}$$

$$\Delta P_{\text{corr}}^{\text{L-J,soft}} = \frac{\Delta U_{\text{corr}}^{\text{L-J,soft}}}{V}, \tag{S26}$$

where $s_c = r_c/\lambda$.

When a hard cutoff is applied to the L-J potential, it is defined by

$$\begin{aligned}&\tilde{u}(r) = u(r)S(r), \\ &S(r) = \begin{cases}1 & r < r_c, \\ 0 & r > r_c.\end{cases}\end{aligned} \tag{S27}$$

The correction terms can be calculated as

$$\frac{\Delta U_{\text{corr}}^{\text{L-J,hard}}}{N} = 2\pi\rho\int_{r_c}^{\infty} \mathrm{d}r\, u(r) r^2, \tag{S28}$$

$$\Delta P_{\text{corr}}^{\text{L-J,hard}} = 2\pi\rho^2\left[\frac{1}{3}u(r_c)r_c^3 + \int_{r_c}^{\infty} \mathrm{d}r\, u(r) r^2\right]. \tag{S29}$$

Similarly, the correction to the potential energy and that to the pressure can be derived by neglecting the r^{-12} term in the L-J potential and assuming $g(r)=1$ beyond the cutoff distance

$$\frac{\Delta U_{\text{corr}}^{\text{L-J,hard}}}{N} = 2\pi\rho \cdot 4 \left(-\frac{\sigma^6}{3r_c^3} \right) \tag{S30}$$

$$\Delta P_{\text{corr}}^{\text{L-J,hard}} = 2\pi\rho^2 \cdot 4 \left(-\frac{2\sigma^6}{3r_c^3} \right) \quad . \tag{S31}$$

Following the same procedure, we can obtain the cutoff corrections for other forms of short-range interactions in real molecular systems.

S1-C: Estimators for Enthalpy, Density, Isobaric Heat Capacity, Isothermal Compressibility, and Thermal Expansion Coefficient.

1) Enthalpy

In classical MD, the enthalpy is estimated by

$$\tilde{H} = \langle \tilde{H}_{\text{ins}} \rangle = \left\langle \frac{1}{2}\mathbf{p}^T\mathbf{M}^{-1}\mathbf{p} + U(\mathbf{x}) + P_{\text{ext}}V \right\rangle. \tag{S32}$$

In PIMD, the primitive estimator for enthalpy is

$$\tilde{H}^{\text{QM}} = \langle \tilde{H}_{\text{prim}}^{\text{QM}} \rangle = \left\langle K_{\text{prim}}^{\text{QM}} + \frac{1}{L}\sum_{i=1}^{L} U(\mathbf{x}_i) + P_{\text{ext}}V \right\rangle, \tag{S33}$$

and the virial estimator is defined as

$$\tilde{H}^{\text{QM}} = \langle \tilde{H}_{\text{vir}}^{\text{QM}} \rangle = \left\langle K_{\text{vir}}^{\text{QM}} + \frac{1}{L}\sum_{i=1}^{L} U(\mathbf{x}_i) + P_{\text{ext}}V \right\rangle, \tag{S34}$$

which satisfies the relation

$$\tilde{H}_{\text{prim}}^{\text{QM}} = \tilde{H}_{\text{vir}}^{\text{QM}} = -\frac{\partial \ln Z_{\text{NPT}}}{\partial \beta}. \tag{S35}$$

In the main text, we use the virial estimator for the enthalpy for better convergence.

2) Density

For the density, the estimator is

$$\rho = \frac{M_{\text{system}}}{\langle V \rangle}. \tag{S36}$$

for both classical and quantum cases. M_{system} is the total mass of the system.

3) Isobaric Heat Capacity

The isobaric heat capacity is defined as

$$C_p = \left(\frac{\partial \tilde{H}}{\partial T} \right)_P , \tag{S37}$$

In classical mechanics, the enthalpy can be calculated throughout the partition function of eq (2) in the main text

$$\tilde{H} = -\frac{\partial \ln Z_{\text{NPT}}}{\partial \beta}. \tag{S38}$$

The isobaric heat capacity can then be calculated as

$$C_p = \frac{\partial}{\partial T}\left(-\frac{\partial \ln Z_{\text{NPT}}}{\partial \beta} \right) = \frac{1}{k_B T^2} \frac{\partial^2 \ln Z_{\text{NPT}}}{\partial \beta^2} = \frac{1}{k_B T^2}\left(\langle \tilde{H}_{\text{ins}}^2 \rangle - \langle \tilde{H}_{\text{ins}} \rangle^2 \right) , \tag{S39}$$

where $\langle \cdot \rangle$ denotes the ensemble average. The isobaric heat capacity is explicitly related to the variance of enthalpy $\sigma_{\tilde{H}}^2 = \langle \tilde{H}_{\text{ins}}^2 \rangle - \langle \tilde{H}_{\text{ins}} \rangle^2$. Equation (S39) can be recast into

$$C_p = \frac{\sigma_{\tilde{H}}^2}{k_B T^2} = \frac{\sigma_K^2}{k_B T^2} + \frac{\sigma_{U+P_{\text{ext}}V}^2}{k_B T^2} \tag{S40}$$

in classical statistical mechanics, where $\sigma_A^2 = \left\langle A^2 \right\rangle - \left\langle A \right\rangle^2$ is the variance of property A.

When PIMD or PIMC is used for quantum statistical mechanics, the classical partition function in eq (S39) should be replaced by that in the path integral formulation[2]. For the

primitive estimator of the enthalpy[1] in eq (S33), the isobaric heat capacity can also be calculated as

$$C_{p,\mathrm{prim}}^{\mathrm{QM}} = \frac{1}{k_B T^2}\frac{\partial^2 \ln Z_{\mathrm{NPT}}}{\partial \beta^2} = \frac{1}{k_B T^2}\left(\langle (\tilde{H}_{\mathrm{prim}}^{\mathrm{QM}})^2 \rangle - \langle \tilde{H}_{\mathrm{prim}}^{\mathrm{QM}} \rangle^2 - \frac{N_f L}{2\beta^2} + \frac{2}{\beta}\langle K_{\mathrm{prim}}^{\mathrm{QM}} \rangle \right). \tag{S41}$$

The last two terms at the right-hand side of eq (S41) are from the derivatives (of the component of the effective potential contributed by the kinetic energy operator) with respect to the Boltzmann factor $\beta = k_B T$.

In addition to the estimator provided in eq (S41), the virial estimator of the enthalpy, eq (S34) can produce a different expression of the isobaric heat capacity[5].

$$C_{p,\mathrm{vir}}^{\mathrm{QM}} = -\frac{1}{k_B T^2}\frac{\partial \left\langle \tilde{H}_{\mathrm{vir}}^{\mathrm{QM}} \right\rangle}{\partial \beta} = \frac{1}{k_B T^2}\left(\langle \tilde{H}_{\mathrm{prim}}^{\mathrm{QM}} \tilde{H}_{\mathrm{vir}}^{\mathrm{QM}} \rangle - \langle \tilde{H}_{\mathrm{prim}}^{\mathrm{QM}} \rangle \langle \tilde{H}_{\mathrm{vir}}^{\mathrm{QM}} \rangle + \frac{N_f}{2\beta^2} \right). \tag{S42}$$

4) Isothermal Compressibility

The isothermal compressibility is defined as

$$\kappa_T = -\frac{1}{V}\left(\frac{\partial V}{\partial P} \right)_T. \tag{S43}$$

In the isobaric-isothermal ensemble, the volume fluctuates and should be replaced by its ensemble average

$$\kappa_T = -\frac{1}{\langle V \rangle}\left(\frac{\partial \langle V \rangle}{\partial P_{\mathrm{ext}}} \right)_T = \frac{\beta}{\langle V \rangle}\left(\langle V^2 \rangle - \langle V \rangle^2 \right). \tag{S44}$$

The isothermal compressibility is expressed in terms of the fluctuation of volume.

In the path integral formulation, as the volume distribution remains the same as in the classical case, the estimator of the isothermal compressibility remains unchanged.

5) Thermal Expansion Coefficient

The thermal expansion coefficient is defined as

$$\alpha = \frac{1}{V}\left(\frac{\partial V}{\partial T}\right)_P . \tag{S45}$$

Likewise, the volume is replaced by the expectation. The estimator in the NPT ensemble can be expressed as

$$\alpha = \frac{1}{\langle V\rangle}\left(\frac{\partial\langle V\rangle}{\partial T}\right) = \frac{1}{k_B T^2\langle V\rangle}\left(\langle V\tilde{H}_{\text{ins}}\rangle - \langle V\rangle\langle\tilde{H}_{\text{ins}}\rangle\right). \tag{S46}$$

In the path integral formulation, the estimator reads

$$\alpha^{\text{QM}} = -\frac{1}{k_B T^2\langle V\rangle}\frac{\partial\langle V\rangle}{\partial\beta} = \frac{1}{k_B T^2\langle V\rangle}\left(\langle V\tilde{H}^{\text{QM}}_{\text{prim}}\rangle - \langle V\rangle\left\langle\tilde{H}^{\text{QM}}_{\text{prim}}\right\rangle\right). \tag{S47}$$

By integration by parts, it can also be expressed in terms of the virial estimator as

$$\alpha^{\text{QM}} = \frac{1}{k_B T^2\langle V\rangle}\left(\langle V\tilde{H}^{\text{QM}}_{\text{prim}}\rangle - \langle V\rangle\langle\tilde{H}^{\text{QM}}_{\text{prim}}\rangle\right) = \frac{1}{k_B T^2\langle V\rangle}\left(\langle V\tilde{H}^{\text{QM}}_{\text{vir}}\rangle - \langle V\rangle\langle\tilde{H}^{\text{QM}}_{\text{vir}}\rangle\right). \tag{S48}$$

6) Explicit Analytical Evaluation of the Component that is a Function of only Momentum in Classical Statistical Mechanics

In classical statistical mechanics, as shown by the distribution function $\exp\left[-\beta\left(PV + H\left(\mathbf{x},\mathbf{p}\right)\right)\right]$ of the isobaric-isothermal ensemble of eq (2) of the main text, the momentum distribution is independent of the distribution of the coordinate and volume. The momentum distribution is simply the Maxwell distribution, a Gaussian distribution of momentum $\exp\left[-\beta\mathbf{p}^T\mathbf{M}^{-1}\mathbf{p}/2\right]$ which is always known without calculation in classical statistical mechanics. Estimation of the enthalpy can be divided into two terms,

$$\tilde{H} = \langle\tilde{H}_{\text{ins}}\rangle = \left\langle\frac{1}{2}\mathbf{p}^T\mathbf{M}^{-1}\mathbf{p}\right\rangle + \left\langle U(\mathbf{x}) + P_{\text{ext}}V\right\rangle = \frac{N_f k_B T}{2} + \left\langle U(\mathbf{x}) + P_{\text{ext}}V\right\rangle. \tag{S49}$$

Estimation of the variance of the enthalpy can be decomposed into two components. The variance of the enthalpy is equivalent to the sum of two parts as

$$\sigma_{\dot{H}}^2 = \sigma_K^2 + \sigma_{U+P_{\text{ext}}V}^2 = \frac{N_f \left(k_B T\right)^2}{2} + \sigma_{U+P_{\text{ext}}V}^2 \quad . \tag{S50}$$

Moreover, in classical statistical mechanics the variance of the kinetic energy σ_K^2 only depends on the Maxwell momentum distribution, which yields $\sigma_K^2 = N_f \left(k_B T\right)^2 / 2$. The contribution of σ_K^2 to the isobaric heat capacity, the first term of the right-hand side of eq (S40), is $N_f k_B / 2$. Equation (S40) then becomes

$$C_p = \frac{N_f k_B}{2} + \frac{\sigma_{U+P_{\text{ext}}V}^2}{k_B T^2} \tag{S51}$$

for the evaluation of the isobaric heat capacity.

Because eq (2) of the main text indicates that the momentum distribution and the volume distribution are independent in the isobaric-isothermal ensemble, the covariance of the kinetic energy and volume is zero. Provided that the Maxwell momentum distribution is known in classical statistical mechanics, eq (S46) for the estimator for the thermal expansion coefficient can be recast into

$$\alpha = \frac{1}{\langle V \rangle} \left(\frac{\partial \langle V \rangle}{\partial T} \right) = \frac{1}{k_B T^2 \langle V \rangle} \left[\langle V \left(U(\mathbf{x}) + P_{\text{ext}} V \right) \rangle - \langle V \rangle \langle U(\mathbf{x}) + P_{\text{ext}} V \rangle \right]. \tag{S52}$$

Such a strategy is not necessary in PIMD or PIMC of quantum statistical mechanics, because all physical properties are functions of only the coordinate of the PI bead and the volume. The momentum of the PI bead is simply fictitious, of which the distribution is not important at all in the evaluation of thermodynamic properties.

S2. Comparison between the "Middle" Schemes with the MTTK Barostat

In the isotropic isobaric-isothermal ensemble, the equilibrium distribution is described by

$$\rho(\mathbf{x},\mathbf{p},V) = \frac{1}{Z_{\mathrm{NPT}}}\exp\left[-\beta\left(\frac{1}{2}\mathbf{p}^T\mathbf{M}^{-1}\mathbf{p} + U(\mathbf{x}) + P_{\mathrm{ext}}V\right)\right] \quad . \tag{S53}$$

When using the MTTK barostat (coupled with the Langevin thermostat) to sample the isobaric-isothermal ensemble, the momentum of fictitious 'piston' is introduced, and the full equations of motion are:

$$\begin{aligned}
\dot{\mathbf{x}} &= \mathbf{M}^{-1}\mathbf{p} + \frac{p_\varepsilon}{W}\mathbf{x} \\
\dot{\mathbf{p}} &= -\frac{\partial U}{\partial \mathbf{x}} - \left(1+\frac{d}{N_f}\right)\frac{p}{W}\mathbf{p} - \gamma_{\mathrm{Lang}}\mathbf{p} + \sqrt{\frac{2\gamma_{\mathrm{Lang}}}{\beta}}\mathbf{M}^{1/2}\boldsymbol{\zeta}(t) \\
\dot{V} &= dV\frac{p_\varepsilon}{W} \\
\dot{p}_\varepsilon &= dV\left(P_{\mathrm{int}} - P_{\mathrm{ext}}\right) + \frac{d}{N_f}\mathbf{p}^T\mathbf{M}^{-1}\mathbf{p} - \gamma^V_{\mathrm{Lang}}p_\varepsilon + \sqrt{\frac{2\gamma^V_{\mathrm{Lang}}}{\beta}}W^{1/2}\zeta_\varepsilon(t)
\end{aligned} \tag{S54}$$

where $\boldsymbol{\zeta}(t)$ and $\zeta_\varepsilon(t)$ represents the Gaussian white noise (vector and scalar variables, respectively). The equations of motion lead to the stationary distribution

$$\rho(\mathbf{x},\mathbf{p},V,p_\varepsilon) = \mathcal{N}_{\mathrm{MTTK}}\exp\left[-\beta\left(\frac{1}{2}\mathbf{p}^T\mathbf{M}^{-1}\mathbf{p} + U(\mathbf{x}) + P_{\mathrm{ext}}V + \frac{p_\varepsilon^2}{2W}\right)\right] \quad , \tag{S55}$$

whose marginal distribution of $\mathbf{x},\mathbf{p},V$ is the equilibrium distribution of the isobaric-isothermal ensemble, eq (S53). In eq (S55), $\mathcal{N}_{\mathrm{MTTK}}$ is a normalization constant.

Below we show that $\rho(\mathbf{x},\mathbf{p},V,p_\varepsilon)$ of eq (S55) is the stationary distribution. The Kolmogorov operators of the decomposition of the MTTK barostat in the main text reads

$$\mathcal{L}_{\mathbf{x}}\rho = -\mathbf{p}^T\mathbf{M}^{-1}\frac{\partial\rho}{\partial\mathbf{x}} = \rho\left(\beta\mathbf{p}^T\mathbf{M}^{-1}\frac{\partial U}{\partial\mathbf{x}}\right), \tag{S56}$$

$$\mathcal{L}_{\mathbf{p}}\rho = \left(\frac{\partial U}{\partial \mathbf{x}}\right)^T \frac{\partial \rho}{\partial \mathbf{p}} = \rho\left(-\beta \mathbf{p}^T \mathbf{M}^{-1} \frac{\partial U}{\partial \mathbf{x}}\right), \tag{S57}$$

$$\mathcal{L}_T \rho = \gamma_{\text{Lang}} \left(\frac{\partial}{\partial \mathbf{p}}\right)^T (\mathbf{p}\rho) + \frac{\gamma_{\text{Lang}}}{\beta} \left(\frac{\partial}{\partial \mathbf{p}}\right)^T \mathbf{M} \frac{\partial \rho}{\partial \mathbf{p}} = 0, \tag{S58}$$

$$\mathcal{L}_{\mathbf{x}_r} \rho = -\frac{p_\varepsilon}{W} \left(\frac{\partial}{\partial \mathbf{x}}\right)^T (\mathbf{x}\rho) = \frac{p_\varepsilon}{W} \rho\left(-N_f + \beta \mathbf{x}^T \frac{\partial U}{\partial \mathbf{x}}\right), \tag{S59}$$

$$\mathcal{L}_{\mathbf{p}_r} \rho = \left(1 + \frac{d}{N_f}\right) \frac{p_\varepsilon}{W} \left(\frac{\partial}{\partial \mathbf{p}}\right)^T (\mathbf{p}\rho) = \left(1 + \frac{d}{N_f}\right) \frac{p_\varepsilon}{W} \rho\left(N_f - \beta \mathbf{p}^T \mathbf{M}^{-1} \mathbf{p}\right), \tag{S60}$$

$$\mathcal{L}_V \rho = -d \frac{p_\varepsilon}{W} \frac{\partial}{\partial V}(V\rho) = d \frac{p_\varepsilon}{W} \rho\left(-1 + \beta P_{\text{ext}} V\right), \tag{S61}$$

$$\begin{aligned} \mathcal{L}_{p_\varepsilon} \rho &= -dV\left(P_{\text{int}} - P_{\text{ext}}\right) \frac{\partial \rho}{\partial p_\varepsilon} - \frac{d}{N_f} \mathbf{p}^T \mathbf{M}^{-1} \mathbf{p} \frac{\partial \rho}{\partial p_\varepsilon} \\ &= \frac{p_\varepsilon}{W} \beta \rho \left[\left(1 + \frac{d}{N_f}\right) \mathbf{p}^T \mathbf{M}^{-1} \mathbf{p} - \mathbf{x}^T \frac{\partial U}{\partial \mathbf{x}} - d P_{\text{ext}} V\right], \end{aligned} \tag{S62}$$

$$\mathcal{L}_B \rho = \gamma_{\text{Lang}}^V \frac{\partial}{\partial p_\varepsilon}(p_\varepsilon \rho) + \frac{\gamma_{\text{Lang}}^V W}{\beta} \frac{\partial^2 \rho}{\partial p_\varepsilon^2} = 0. \tag{S63}$$

The distribution function $\rho(\mathbf{x}, \mathbf{p}, V, p_\varepsilon)$ of eq (S55) is substituted in the right-hand side of each of eqs (S56)-(S63). Equations (S56)-(S63) lead to

$$\mathcal{L}_{\text{MTTK}}^{(\text{full})} \rho \equiv \left(\mathcal{L}_{\mathbf{x}} + \mathcal{L}_{\mathbf{x}_r} + \mathcal{L}_{\mathbf{p}} + \mathcal{L}_{\mathbf{p}_r} + \mathcal{L}_V + \mathcal{L}_{p_\varepsilon} + \mathcal{L}_T + \mathcal{L}_B\right) \rho = 0, \tag{S64}$$

where the left-hand side of eq (S64) is the Liouville equation of the MTTK barostat and the right-hand side of eq (S64) indicates that $\rho(\mathbf{x}, \mathbf{p}, V, p_\varepsilon)$ of eq (S55) is the stationary distribution. One can also verify that $\rho(\mathbf{x}, \mathbf{p}, V, p_\varepsilon)$ of eq (S55) is the stationary distribution by employing the conserve quantity and non-compressibility of the MTTK barostat as demonstrated in ref [6].

In the main text we describe that the efficient integrator for the isobaric-isothermal ensemble should approach the "middle" thermostat scheme for the canonical ensemble when barostat

effectively vanishes. The recommended "middle" scheme for the MTTK barostat in the main text is only one possible choice. Here, we investigate several possible alternative decomposition schemes with numerical tests to show that the recommended "middle" scheme (proposed in the main text) is actually the optimal decomposition.

To identity the major aspect of the decomposition order, we introduce

$$\mathcal{L}_{\mathbf{x}_t} = \mathcal{L}_{\mathbf{x}} + \mathcal{L}_{\mathbf{x}_r} \tag{S65}$$

and

$$\mathcal{L}_{\mathbf{p}_t} = \mathcal{L}_{\mathbf{p}} + \mathcal{L}_{\mathbf{p}_r} \quad , \tag{S66}$$

which is closely related to the decomposition proposed in ref [7]. That is,

$$\mathcal{L}_{\mathbf{x}_t}\rho = -N_f \frac{p_\varepsilon}{W}\rho - \left(\mathbf{p}^T\mathbf{M}^{-1} + \frac{p_\varepsilon}{W}\mathbf{x}^T\right)\frac{\partial\rho}{\partial\mathbf{x}} \tag{S67}$$

and

$$\mathcal{L}_{\mathbf{p}_t}\rho = \left(\frac{\partial U}{\partial\mathbf{x}} + \left(1+\frac{d}{N_f}\right)\frac{p_\varepsilon}{W}\mathbf{p}\right)^T\frac{\partial\rho}{\partial\mathbf{p}} + \left(N_f + d\right)\frac{p_\varepsilon}{W}\rho \quad . \tag{S68}$$

The relevant Kolmogorov operators are defined by eqs (S67), (S68), (S58), (S61), (S62), and (S63). Further comparison of this strategy to the decomposition in the main text (with eqs (S56) -(S63)) is presented in Sub-Section **S2-C**.

The commutation relations between different Kolmogorov operators read

$$\begin{aligned}
&\left[\mathcal{L}_{\mathbf{x}_t}, \mathcal{L}_V\right] = 0 \\
&\left[\mathcal{L}_{\mathbf{p}_t}, \mathcal{L}_V\right] = 0 \\
&\left[\mathcal{L}_T, \mathcal{L}_V\right] = 0 \\
&\left[\mathcal{L}_T, \mathcal{L}_B\right] = 0
\end{aligned} \quad . \tag{S69}$$

By applying these rules and considering the fact that the "p – x – T – x – p" scheme (based on the

velocity-Verlet algorithm) is the optimal decomposition for the canonical ensemble[8-11], we have 6 alternatives with the MTTK barostat, which approaches the "$\mathrm{p-x-T-x-p}$" scheme[8, 10, 11] (based on the velocity-Verlet algorithm) when the barastat is withdrew.

We simplify the notation by considering the symmetry of the evolution. Only the first half of the propagation (in the right-to-left sequence in the whole integrator for a finite time interval) is utilized for notation. For example, the scheme

$$\begin{aligned} e^{\mathcal{L}_{\mathrm{NPT}}\Delta t} &= e^{\mathcal{L}_{p_\varepsilon}\Delta t/2}e^{\mathcal{L}_V\Delta t/2}e^{\mathcal{L}_{\mathbf{p}_t}\Delta t/2}e^{\mathcal{L}_{\mathbf{x}_t}\Delta t/2}e^{\mathcal{L}_T\Delta t}e^{\mathcal{L}_B\Delta t}e^{\mathcal{L}_{\mathbf{x}_t}\Delta t/2}e^{\mathcal{L}_{\mathbf{p}_t}\Delta t/2}e^{\mathcal{L}_V\Delta t/2}e^{\mathcal{L}_{p_\varepsilon}\Delta t/2} \\ &= e^{\mathcal{L}_{p_\varepsilon}\Delta t/2}e^{\mathcal{L}_V\Delta t/2}e^{\mathcal{L}_{\mathbf{p}_t}\Delta t/2}e^{\mathcal{L}_{\mathbf{x}_t}\Delta t/2}e^{\mathcal{L}_B\Delta t/2}e^{\mathcal{L}_T\Delta t/2}e^{\mathcal{L}_T\Delta t/2}e^{\mathcal{L}_B\Delta t/2}e^{\mathcal{L}_{\mathbf{x}_t}\Delta t/2}e^{\mathcal{L}_{\mathbf{p}_t}\Delta t/2}e^{\mathcal{L}_V\Delta t/2}e^{\mathcal{L}_{p_\varepsilon}\Delta t/2} \end{aligned} \tag{S70}$$

is denoted as $\mathrm{T-B-x-p-V-p_V}$. The six velocity-Verlet-based "middle" schemes are listed in

Table S1, and the corresponding schemes based on the leap-frog algorithm are listed in **Table S2**.

Table S1. Tested "Middle" Schemes Based on the Velocity-Verlet Algorithm with the MTTK Barostat

#	Decomposition Order	Simplified notation
#1	$e^{\mathcal{L}_{p_\varepsilon}\Delta t/2}e^{\mathcal{L}_V\Delta t/2}e^{\mathcal{L}_{\mathbf{p}_t}\Delta t/2}e^{\mathcal{L}_{\mathbf{x}_t}\Delta t/2}e^{\mathcal{L}_T\Delta t}e^{\mathcal{L}_B\Delta t}e^{\mathcal{L}_{\mathbf{x}_t}\Delta t/2}e^{\mathcal{L}_{\mathbf{p}_t}\Delta t/2}e^{\mathcal{L}_V\Delta t/2}e^{\mathcal{L}_{p_\varepsilon}\Delta t/2}$	$\mathrm{T-B-x-p-V-p_V}$
#2	$e^{\mathcal{L}_V\Delta t/2}e^{\mathcal{L}_{p_\varepsilon}\Delta t/2}e^{\mathcal{L}_{\mathbf{p}_t}\Delta t/2}e^{\mathcal{L}_{\mathbf{x}_t}\Delta t/2}e^{\mathcal{L}_T\Delta t}e^{\mathcal{L}_B\Delta t}e^{\mathcal{L}_{\mathbf{x}_t}\Delta t/2}e^{\mathcal{L}_{\mathbf{p}_t}\Delta t/2}e^{\mathcal{L}_{p_\varepsilon}\Delta t/2}e^{\mathcal{L}_V\Delta t/2}$	$\mathrm{T-B-x-p-p_V-V}$
#3	$e^{\mathcal{L}_{\mathbf{p}_t}\Delta t/2}e^{\mathcal{L}_{\mathbf{x}_t}\Delta t/2}e^{\mathcal{L}_{p_\varepsilon}\Delta t/2}e^{\mathcal{L}_V\Delta t/2}e^{\mathcal{L}_T\Delta t}e^{\mathcal{L}_B\Delta t}e^{\mathcal{L}_V\Delta t/2}e^{\mathcal{L}_{p_\varepsilon}\Delta t/2}e^{\mathcal{L}_{\mathbf{x}_t}\Delta t/2}e^{\mathcal{L}_{\mathbf{p}_t}\Delta t/2}$	$\mathrm{T-B-V-p_V-x-p}$
#4	$e^{\mathcal{L}_{\mathbf{p}_t}\Delta t/2}e^{\mathcal{L}_{\mathbf{x}_t}\Delta t/2}e^{\mathcal{L}_V\Delta t/2}e^{\mathcal{L}_{p_\varepsilon}\Delta t/2}e^{\mathcal{L}_T\Delta t}e^{\mathcal{L}_B\Delta t}e^{\mathcal{L}_{p_\varepsilon}\Delta t/2}e^{\mathcal{L}_V\Delta t/2}e^{\mathcal{L}_{\mathbf{x}_t}\Delta t/2}e^{\mathcal{L}_{\mathbf{p}_t}\Delta t/2}$	$\mathrm{T-B-p_V-V-x-p}$
#5	$e^{\mathcal{L}_{\mathbf{p}_t}\Delta t/2}e^{\mathcal{L}_{p_\varepsilon}\Delta t/2}e^{\mathcal{L}_V\Delta t/2}e^{\mathcal{L}_{\mathbf{x}_t}\Delta t/2}e^{\mathcal{L}_T\Delta t}e^{\mathcal{L}_B\Delta t}e^{\mathcal{L}_{\mathbf{x}_t}\Delta t/2}e^{\mathcal{L}_V\Delta t/2}e^{\mathcal{L}_{p_\varepsilon}\Delta t/2}e^{\mathcal{L}_{\mathbf{p}_t}\Delta t/2}$	$\mathrm{T-B-x-V-p_V-p}$
#6	$e^{\mathcal{L}_{\mathbf{p}_t}\Delta t/2}e^{\mathcal{L}_V\Delta t/2}e^{\mathcal{L}_{p_\varepsilon}\Delta t/2}e^{\mathcal{L}_{\mathbf{x}_t}\Delta t/2}e^{\mathcal{L}_T\Delta t}e^{\mathcal{L}_B\Delta t}e^{\mathcal{L}_{\mathbf{x}_t}\Delta t/2}e^{\mathcal{L}_{p_\varepsilon}\Delta t/2}e^{\mathcal{L}_V\Delta t/2}e^{\mathcal{L}_{\mathbf{p}_t}\Delta t/2}$	$\mathrm{T-B-x-p_V-V-p}$

Table S2. Tested "Middle" Schemes Based on the Leap-frog Algorithm with the MTTK Barostat

#	Decomposition Order	Simplified notation
#1	$e^{\mathcal{L}_{\mathbf{x}_t}\Delta t/2}e^{\mathcal{L}_T\Delta t}e^{\mathcal{L}_B\Delta t}e^{\mathcal{L}_{\mathbf{x}_t}\Delta t/2}e^{\mathcal{L}_{\mathbf{p}_t}\Delta t/2}e^{\mathcal{L}_V\Delta t/2}e^{\mathcal{L}_{p_\varepsilon}\Delta t}e^{\mathcal{L}_V\Delta t/2}e^{\mathcal{L}_{\mathbf{p}_t}\Delta t/2}$	$\mathrm{T}-\mathrm{B}-\mathrm{x}-\mathrm{p}-\mathrm{V}-\mathrm{p}_\mathrm{V}$
#2	$e^{\mathcal{L}_{\mathbf{x}_t}\Delta t/2}e^{\mathcal{L}_T\Delta t}e^{\mathcal{L}_B\Delta t}e^{\mathcal{L}_{\mathbf{x}_t}\Delta t/2}e^{\mathcal{L}_{\mathbf{p}_t}\Delta t/2}e^{\mathcal{L}_{p_\varepsilon}\Delta t/2}e^{\mathcal{L}_V\Delta t}e^{\mathcal{L}_{p_\varepsilon}\Delta t/2}e^{\mathcal{L}_{\mathbf{p}_t}\Delta t/2}$	$\mathrm{T}-\mathrm{B}-\mathrm{x}-\mathrm{p}-\mathrm{p}_\mathrm{V}-\mathrm{V}$
#3	$e^{\mathcal{L}_{\mathbf{x}_t}\Delta t/2}e^{\mathcal{L}_{p_\varepsilon}\Delta t/2}e^{\mathcal{L}_V\Delta t/2}e^{\mathcal{L}_T\Delta t}e^{\mathcal{L}_B\Delta t}e^{\mathcal{L}_V\Delta t/2}e^{\mathcal{L}_{p_\varepsilon}\Delta t/2}e^{\mathcal{L}_{\mathbf{x}_t}\Delta t/2}e^{\mathcal{L}_{\mathbf{p}_t}\Delta t}$	$\mathrm{T}-\mathrm{B}-\mathrm{V}-\mathrm{p}_\mathrm{V}-\mathrm{x}-\mathrm{p}$
#4	$e^{\mathcal{L}_{\mathbf{x}_t}\Delta t/2}e^{\mathcal{L}_V\Delta t/2}e^{\mathcal{L}_{p_\varepsilon}\Delta t/2}e^{\mathcal{L}_T\Delta t}e^{\mathcal{L}_B\Delta t}e^{\mathcal{L}_{p_\varepsilon}\Delta t/2}e^{\mathcal{L}_V\Delta t/2}e^{\mathcal{L}_{\mathbf{x}_t}\Delta t/2}e^{\mathcal{L}_{\mathbf{p}_t}\Delta t}$	$\mathrm{T}-\mathrm{B}-\mathrm{p}_\mathrm{V}-\mathrm{V}-\mathrm{x}-\mathrm{p}$
#5	$e^{\mathcal{L}_{p_\varepsilon}\Delta t/2}e^{\mathcal{L}_V\Delta t/2}e^{\mathcal{L}_{\mathbf{x}_t}\Delta t/2}e^{\mathcal{L}_T\Delta t}e^{\mathcal{L}_B\Delta t}e^{\mathcal{L}_{\mathbf{x}_t}\Delta t/2}e^{\mathcal{L}_V\Delta t/2}e^{\mathcal{L}_{p_\varepsilon}\Delta t/2}e^{\mathcal{L}_{\mathbf{p}_t}\Delta t}$	$\mathrm{T}-\mathrm{B}-\mathrm{x}-\mathrm{V}-\mathrm{p}_\mathrm{V}-\mathrm{p}$
#6	$e^{\mathcal{L}_V\Delta t/2}e^{\mathcal{L}_{p_\varepsilon}\Delta t/2}e^{\mathcal{L}_{\mathbf{x}_t}\Delta t/2}e^{\mathcal{L}_T\Delta t}e^{\mathcal{L}_B\Delta t}e^{\mathcal{L}_{\mathbf{x}_t}\Delta t/2}e^{\mathcal{L}_{p_\varepsilon}\Delta t/2}e^{\mathcal{L}_V\Delta t/2}e^{\mathcal{L}_{\mathbf{p}_t}\Delta t}$	$\mathrm{T}-\mathrm{B}-\mathrm{x}-\mathrm{p}_\mathrm{V}-\mathrm{V}-\mathrm{p}$

Scheme **#1** has been proposed in ref [12], although the dynamics in ref [12] is not based on the equations of the MTTK barostat. As will be demonstrated in numerical tests below, its corresponding algorithm in the MTTK barostat analog does NOT considerably outperform the conventional "side" scheme.

In the following sub-sections, we test these six schemes with different benchmark models to identify the best option for MD simulations of the isobaric-isothermal ensemble.

S2-A: Numerical Tests of Different "Middle" Schemes on the One-dimensional Nanowire Model

In this sub-section, we test the proposed schemes listed in Table S1 and Table S2. We utilize the one-dimensional nanowire model of ref [2]. It involves a single particle moving within a one-dimensional cosine potential,

$$U(x,V)=\frac{m\omega^2V^2}{4\pi^2}\left[1-\cos\left(\frac{2\pi x}{V}\right)\right] \quad , \tag{S71}$$

where $m=1$, $\omega=1$. Classical MD simulations of the isobaric-isothermal ensemble are performed at $k_BT=0.01$, and $P_{\text{ext}}=0.01$, and the "piston mass" is set to $W=1000$, where all parameters and variables are in reduced units. Six proposed velocity-Verlet-based "middle" schemes listed in Table S1 and their corresponding leap-frog-based schemes are tested. For each scheme, we run 20 independent trajectories for the model system. After each trajectory is equilibrated for 2×10^7 r.u., it is propagated for 8×10^7 r.u. to evaluate physical properties. The friction parameter γ_{Lang} for the Langevin thermostat and γ^V_{Lang} for the barostat are 1.0 r.u. and 0.001 r.u., respectively. The number of degrees of freedom (N_f) is 1 for this model system.

MD simulations for the 1-dimensional nanowire model of eq (S71) are performed with different time intervals. In Figures S1-S2, eqs (S36) and (S44) are used to calculate the density and isothermal compressibility, and eqs (S32), (S51), and (S46) are utilized to evaluate the enthalpy, isobaric heat capacity, and thermal expansion coefficient. In Figure S3, both eq (S39) and eq (S51) are employed for the evaluation of the isobaric heat capacity.

As shown in **Figure S1**, the length (volume in the 1-dimensional case), potential energy, enthalpy, isobaric heat capacity, isothermal compressibility and thermal expansion coefficient are plotted as functions of the time interval. The gray horizontal lines represent accurate values

obtained by numerical integration. As the time interval decreases, all the schemes converge to the same result, which is consistent with the fact that all integrators are in principle equivalent when the time interval is infinitesimal.

Schemes **#1** and **#2** yield nearly identical numerical results for either velocity-Verlet based schemes or leap-frog based schemes. Schemes **#3** and **#4** also perform nearly the same. Similarly, Schemes **#5** and **#6** produce almost indistinguishable results. This indicates that, although operators $e^{\mathcal{L}_V \Delta t}$ and $e^{\mathcal{L}_{p_\varepsilon} \Delta t}$ do not commute, their relative order in the sequence of the full evolution propagator is not important. Regardless of whether the relative order is '… $\mathrm{p_V - V}$ …' or '… $\mathrm{V - p_V}$ …', it generates almost the same numerical results within the statistical error bar.

Figure S1 suggest that Schemes **#5** and **#6** based on the velocity-Verlet algorithm produce relatively accurate results for the volume and isothermal compressibility at a relatively large time interval. When $\Delta t = 1.0$ r.u. is used, the absolute deviation of the length for these two schemes is only ~ 0.001 r.u., while that of the other four schemes is more than 0.1 r.u.; the absolute deviation of the isothermal compressibility of these two schemes is only ~ 0.5 r.u., and in comparison, those of the other four schemes are more than 7 r.u.. These imply that Schemes **#5** and **#6** are much better for sampling the volume distribution. Moreover, Schemes **#5** and **#6** also perform better for sampling the coordinate distribution, as indicated by the results for the potential energy as a function of the time interval in Panel (b) of Figure S1.

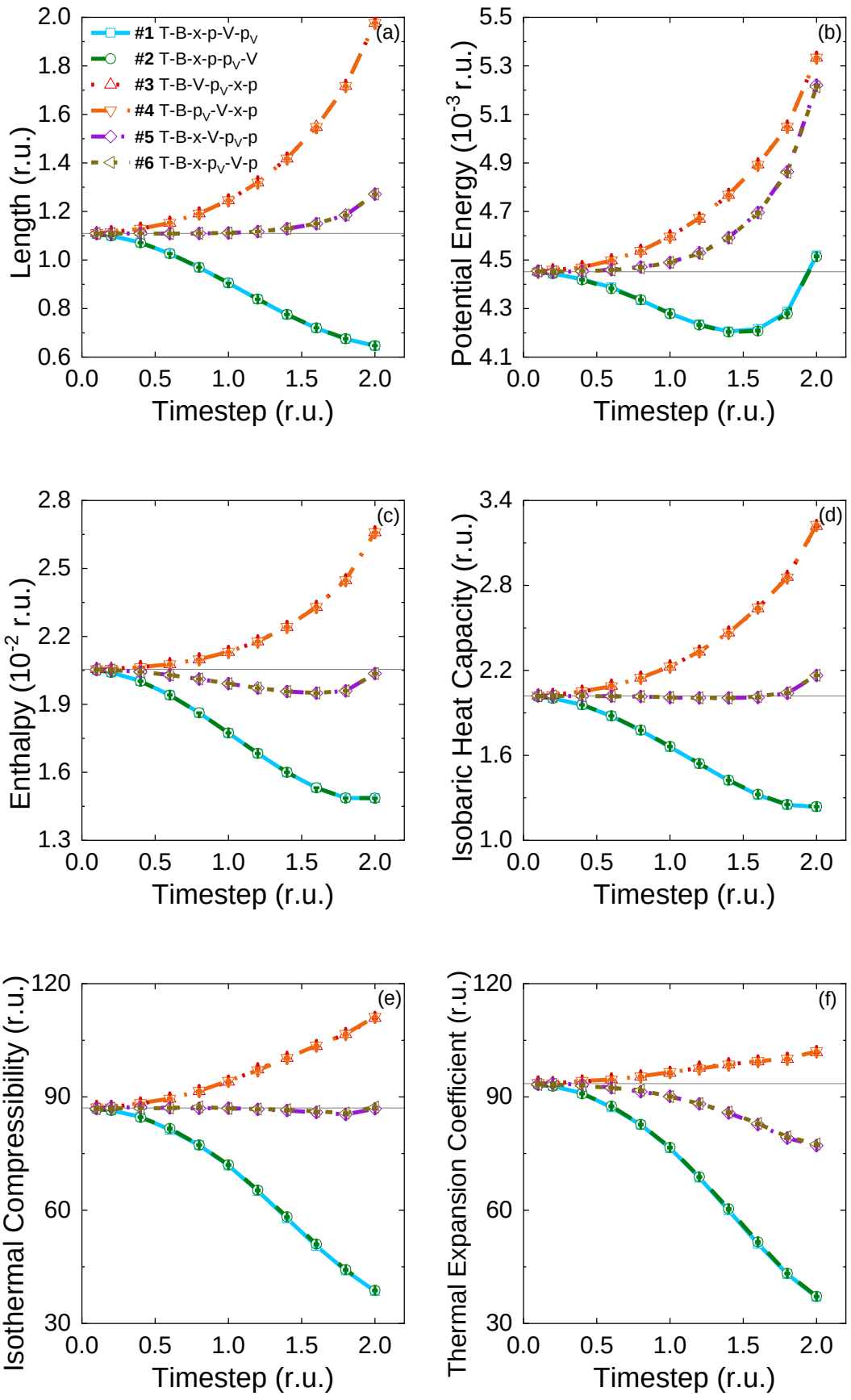
#1 T-B-x-p-V-p$_V$
#2 T-B-x-p-p$_V$-V
#3 T-B-V-p$_V$-x-p
#4 T-B-p$_V$-V-x-p
#5 T-B-x-V-p$_V$-p
#6 T-B-x-p$_V$-V-p
(a)
Length (r.u.)
Timestep (r.u.)
(b)
Potential Energy (10^{-3} r.u.)
Timestep (r.u.)
(c)
Enthalpy (10^{-2} r.u.)
Timestep (r.u.)
(d)
Isobaric Heat Capacity (r.u.)
Timestep (r.u.)
(e)
Isothermal Compressibility (r.u.)
Timestep (r.u.)
(f)
Thermal Expansion Coefficient (r.u.)
Timestep (r.u.)

Figure S1. Comparison of different velocity-Verlet-based "middle" schemes with the MTTK barostat using the one-dimensional nanowire model at $k_B T = 0.01\,\text{r.u.}$ and $P_{\text{ext}} = 0.01\,\text{r.u.}$. The calculated thermodynamic properties include (a) length, (b) potential energy, (c) enthalpy, (d) isobaric heat capacity, (e) isothermal compressibility, and (f) thermal expansion coefficient. Each line corresponds to one scheme listed in Table S1. Gray horizontal lines: accurate values calculated by numerical integration. 20 trajectories for each scheme are equilibrated for 2×10^7 r.u. equilibration and then propagated for 8×10^7 r.u.. All data are divided into 20 groups to calculate the standard error. The friction parameter γ_{Lang} for the Langevin thermostat and γ^V_{Lang} for the barostat are $1.0\,\text{r.u.}$ and $0.001\,\text{r.u.}$, respectively. All MD simulations are performed by our independently developed MD/PIMD program.

The conclusion is similar when the corresponding six schemes based on the leap-frog algorithm are applied. Figure S2 shows that leap-frog-based schemes **#5** and **#6** of Table S2 have the best performance among all six schemes. As described in refs [8, 13], in comparison to the velocity-Verlet-based "middle" thermostat scheme, the leap-frog-based "middle" thermostat scheme generates the more accurate momentum marginal distribution of the canonical ensemble. As expected, leap-frog-based schemes **#5** and **#6** of **Table S2** and **Figure S2** produce better results for the kinetic energy, enthalpy, and thermal expansion coefficient than velocity-Verlet-based schemes **#5** and **#6** of

Table S1 and **Figure S1**. The comparison of **Figure S1**(c) to **Figure S2**(c) demonstrates that, when $\Delta t = 1.0\,\text{r.u.}$ is used, the absolute deviation in the enthalpy generated by velocity-Verlet-

based schemes **#5** and **#6** is $\sim 6\times10^{-4}$ r.u., while that by leap-frog-based schemes **#5** and **#6** is only $\sim 6\times10^{-5}$ r.u., about an order of magnitude smaller. **Figure S1**(f) shows that the absolute deviation in the thermal expansion coefficient produced by velocity-Verlet-based schemes **#5** and **#6** is ~ 3.2 r.u., but **Figure S2**(f) demonstrates that by leap-frog-based schemes **#5** and **#6** is as small as ~ 0.46 r.u..

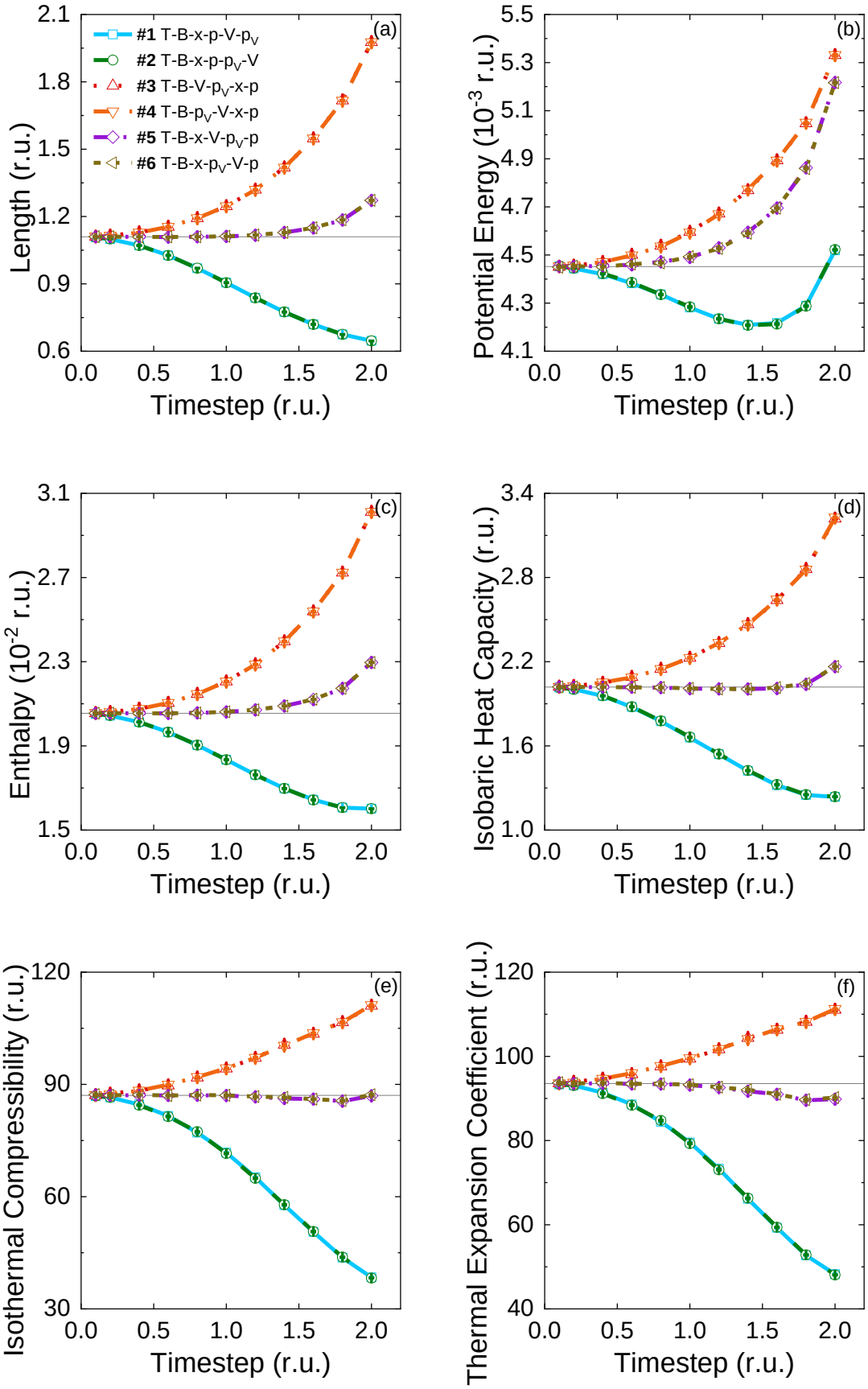
(a)
#1 T-B-x-p-V-p$_V$
#2 T-B-x-p-p$_V$-V
#3 T-B-V-p$_V$-x-p
#4 T-B-p$_V$-V-x-p
#5 T-B-x-V-p$_V$-p
#6 T-B-x-p$_V$-V-p
Length (r.u.)
Timestep (r.u.)
(b)
Potential Energy (10^{-3} r.u.)
Timestep (r.u.)
(c)
Enthalpy (10^{-2} r.u.)
Timestep (r.u.)
(d)
Isobaric Heat Capacity (r.u.)
Timestep (r.u.)
(e)
Isothermal Compressibility (r.u.)
Timestep (r.u.)
(f)
Thermal Expansion Coefficient (r.u.)
Timestep (r.u.)

Figure S2. Comparison of different leap-frog-based schemes with the MTTK barostat using the one-dimensional nanowire model at $k_B T = 0.01\,\text{r.u.}$ and $P_{\text{ext}} = 0.01\,\text{r.u.}$. The calculated thermodynamic properties include (a) length, (b) potential energy, (c) enthalpy, (d) isobaric heat Capacity, (e) isothermal compressibility and (f) thermal expansion coefficient. Each line corresponds to one scheme listed in **Table S2**. Gray horizontal lines: accurate values calculated by numerical integration. 20 trajectories for each scheme are equilibrated for 2×10^7 r.u., then propagated for 8×10^7 r.u. for estimating physical properties. All data are divided into 20 groups to calculate the standard error. The friction parameter γ_{Lang} for the Langevin thermostat and γ^V_{Lang} for the barostat are $1.0\,\text{r.u.}$ and $0.001\,\text{r.u.}$, respectively. All MD simulations are performed by our independently developed MD/PIMD program.

Both classical MD simulations in **Figure S1** for the velocity-Verlet-based schemes and those in **Figure S12** for leap-frog-based schemes employ eq (S51) for the isobaric heat capacity. When the brute-force estimator of eq (S39) is used to evaluate the isobaric heat capacity, it leads significantly worse results. **Figure S3** shows that, when eq (S39) is used for the evaluation of the isobaric heat capacity, velocity-Verlet-based schemes **#5** and **#6**, as well as leap-frog-based schemes **#5** and **#6**, lead to the absolute deviation no smaller than $0.26\,\text{r.u.}$ at $\Delta t = 1.4\,\text{r.u.}$. In comparison, when the estimator of eq (S51) is employed, the absolute deviation of the isobaric heat capacity is only $\sim 0.013\,\text{r.u.}$ at $\Delta t = 1.4\,\text{r.u.}$.

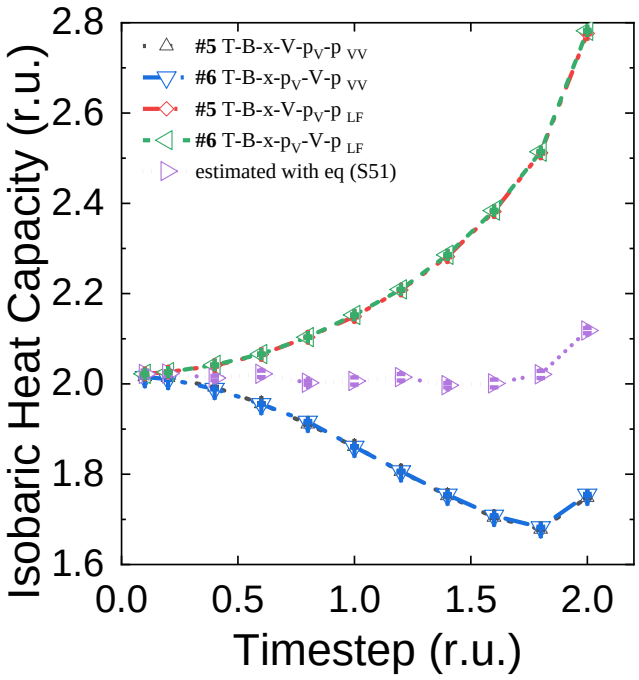

Figure S3. The isobaric heat capacity calculated by the estimator of eq (S51) is compared to that computed by eq (S39), for leap-frog-based schemes **#5** and **#6**, as well as velocity-Verlet-based schemes **#5** and **#6**. Simulation details are similar to those of **Figures S1 and S2**.

Figures S1-S3 suggest that, in the evaluation of physical properties in classical statistical mechanics, we should take full advantage of the known Maxwell momentum distribution and replace the components that are functions of only momentum by the exact averaged results, as described in Sub-Section S1C-6. In the main text as well as the rest of the Supporting Information, while we employ eqs (S36) and (S44) for calculating the density and isothermal compressibility, we use eqs (S49), (S51), and (S52) for the evaluation of the enthalpy, isobaric heat capacity, and thermal expansion coefficient.

We test the performance of different "middle" schemes for liquid water at $T = 298.15\,\mathrm{K}$ and $P_{\mathrm{ext}} = 1\,\mathrm{bar}$ described in the main text is used to compare the different schemes. The flexible q-SPC/fw model is used for the MD simulations. The results show the comparison of six leap-frog-based "middle" schemes with different time intervals. Schemes #5 and #6 perform best in all 6 leap-frog-based schemes, which is consistent with the conclusion based on the results of the nanowire system. Figure S4 of the MD simulations of liquid water also shows that the relative order between the $\mathrm{p_V}$-updating step ($e^{\mathcal{L}_{p_\varepsilon}\Delta t}$) and the V-updating step ($e^{\mathcal{L}_V\Delta t}$) does not noticeably change the results, i.e., the scheme with '… $\mathrm{p_V} - \mathrm{V}$ …' and the counterpart with '… $\mathrm{V} - \mathrm{p_V}$ …' generate similar results within the statistical error bar. One can also verify that Schemes #5 and #6 are also the optimal choice among six velocity-Verlet-based "middle" schemes.

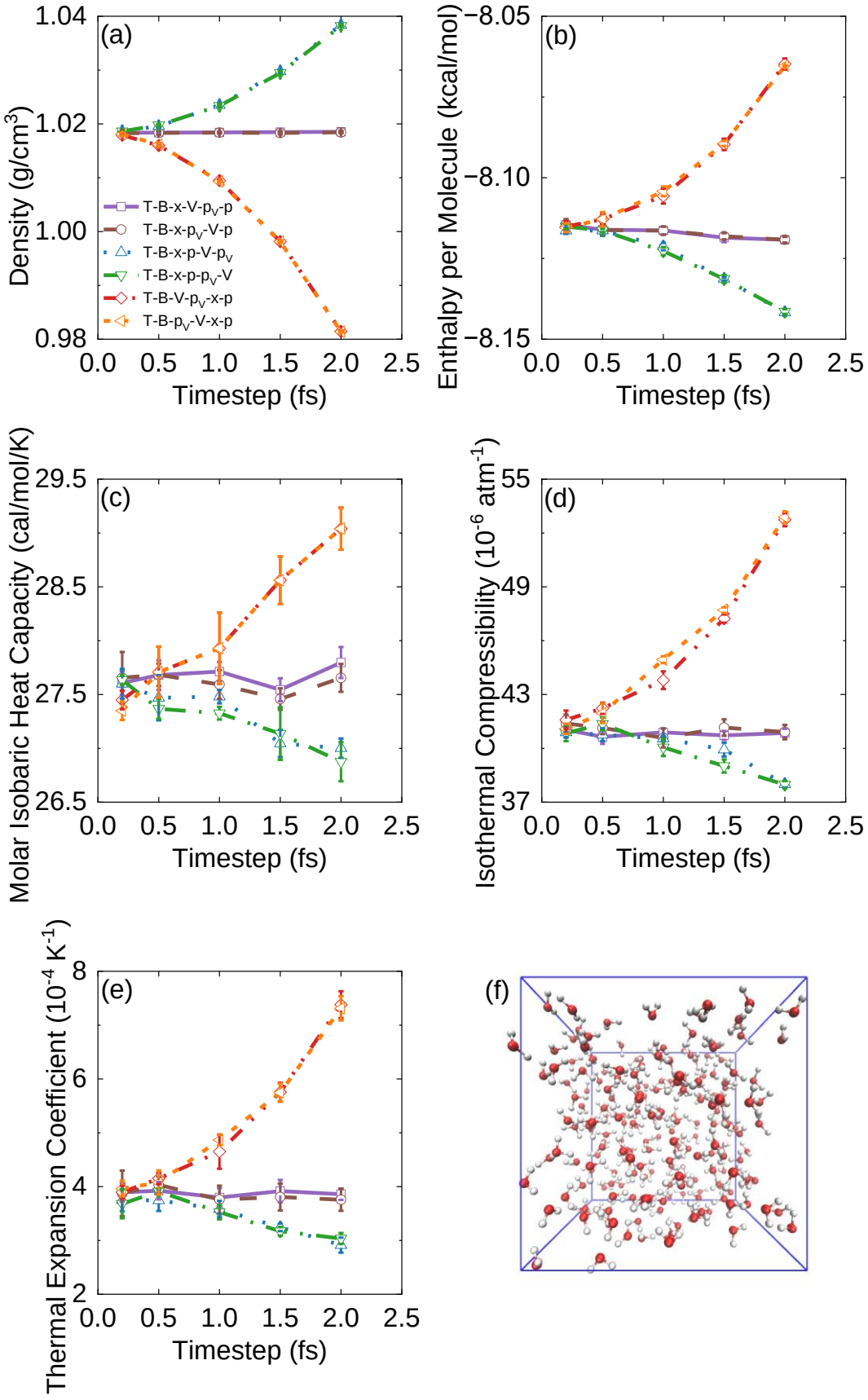
(a)
Density (g/cm^3)
1.04
1.02
1.00
0.98
T-B-x-V-p$_V$-p
T-B-x-p$_V$-V-p
T-B-x-p-V-p$_V$
T-B-x-p-p$_V$-V
T-B-V-p$_V$-x-p
T-B-p$_V$-V-x-p
0.0 0.5 1.0 1.5 2.0 2.5
Timestep (fs)
(b)
Enthalpy per Molecule (kcal/mol)
−8.05
−8.10
−8.15
0.0 0.5 1.0 1.5 2.0 2.5
Timestep (fs)
(c)
Molar Isobaric Heat Capacity (cal/mol/K)
29.5
28.5
27.5
26.5
0.0 0.5 1.0 1.5 2.0 2.5
Timestep (fs)
(d)
Isothermal Compressibility (10^{-6} atm^{-1})
55
49
43
37
0.0 0.5 1.0 1.5 2.0 2.5
Timestep (fs)
(e)
Thermal Expansion Coefficient (10^{-4} K^{-1})
8
6
4
2
0.0 0.5 1.0 1.5 2.0 2.5
Timestep (fs)
(f)

Figure S4. Comparison of different leap-frog-based "middle" schemes with the MTTK barostat using liquid water at $T = 298.15\,\mathrm{K}$ and $P_{\mathrm{ext}} = 1\,\mathrm{atm}$. The q-SPC/fw model is used. The calculated thermodynamic properties include (a) density, (b) enthalpy per molecule (c) molar isobaric heat capacity, (d) isothermal compressibility and (e) thermal expansion coefficient. Each line corresponds to one scheme listed in **Table S2**. Twenty trajectories are equilibrated for 1 ns and propagated for 10 ns, using a cubic box with periodic boundary conditions containing 216 molecules. All data are divided into 20 groups to calculate the standard error. The friction parameter γ_{Lang} for the Langevin thermostat and $\gamma^{V}_{\mathrm{Lang}}$ for the barostat are all $5.0\,\mathrm{ps}^{-1}$, respectively. The "piston" mass W is set to the recommended value as shown in eq (24) in the main text. The cutoff for the short-range interactions is 9 Å. All MD simulations are performed by our modified DL_POLY_2 package[14]. Panel (f) is a snapshot of 216 water molecules in a cubic box with periodic boundary conditions.

S2-C: On Different Decompositions of Kolmogorov Operators of the MTTK Barostat

In the previous sub-sections of Section S2, our theoretical analysis and numerical tests are based on the integrators for the relevant Kolmogorov operators defined by eqs (S67), (S68), (S58), (S61), (S62), and (S63), which are similar to those used in the original version of the MTTK barostat proposed in ref [15]. We focus on the optimal version of the "middle" scheme, Scheme #5 of Table S1. Because the integration of $\mathcal{L}_{\mathbf{x}_t}$ (of eq (S67)) is related to a hyper-sine function[16], we denote it the "middle-sinh" decomposition.

In refs [17, 18], however, it is suggested that in the isobaric-isothermal ensemble, the propagation of extended variables should be separated from the Hamiltonian dynamics of particles. Such a

perspective indicates that the operators or integrators related to the barostat can be identified as the barostat terms, which can be combined to be treated as a whole part so that a clean-cut unified form can be developed. This is indeed what is employed in the main text. When the MTTK barostat is used in the main text, the relevant Kolmogorov operators are defined by eqs (S56)-(S63) instead. The algorithm described in Figure 2 of the main text is similar to Scheme **#5** in Table S2 and can be labeled as '$p_r - p_V - V - x_r - B - x - T - x - B - x_r - V - p_V - p_r - p$' in the right-to-left sequence based on the leap-frog algorithm. Because the integration of $\mathcal{L}_{\mathbf{x}_r}$ (of eq (S59)) involves an exponential function, we denote it the "middle-exp" decomposition.

In this sub-section, we directly compare the performance of the "middle-sinh" decomposition to that of the "middle-exp" decomposition used in the main text. Since the time scale of the variables of the 'barostat' terms is much slower than that of the motion of the particles/atoms as suggested by ref [17], the two decompositions should lead to almost the same results in numerical simulations of real molecular systems. The two decompositions are rigorously equivalent in the limit $W \to \infty$.

Figure S5 shows the simulation results of the two decompositions for the Lennard-Jones liquid. The results for the "middle-exp" decomposition and the "middle-sinh" decomposition are nearly the same in the statistical error bar for each property. It is consistent with our analysis. Because the "middle-exp" decomposition leads to a clean and clear form for implementing any extended-system barostatting methods, we recommend it as the optimal scheme in the main text.

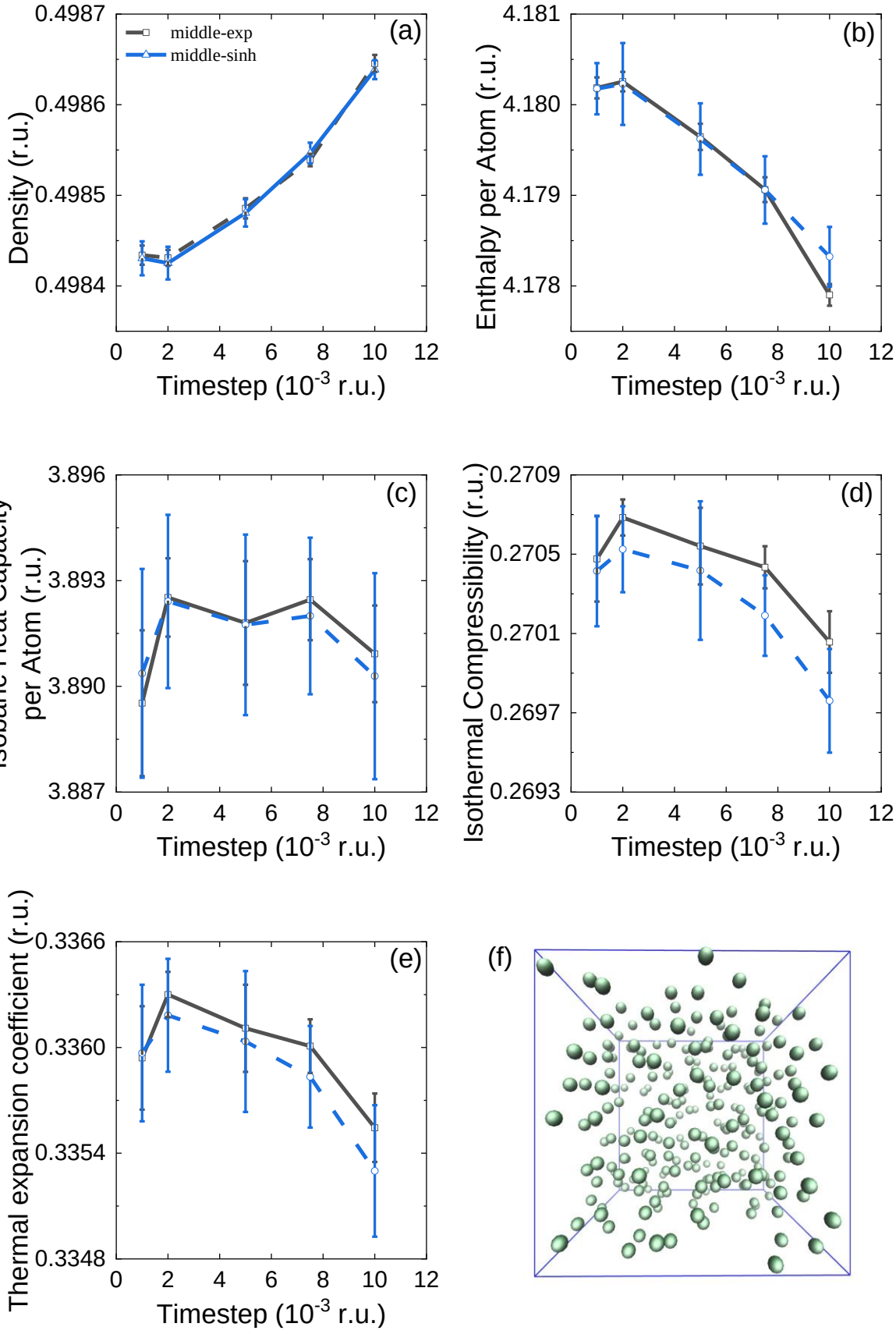
(a)
middle-exp
middle-sinh
Density (r.u.)
0.4987
0.4986
0.4985
0.4984
Timestep (10^{-3} r.u.)
(b)
Enthalpy per Atom (r.u.)
4.181
4.180
4.179
4.178
Timestep (10^{-3} r.u.)
(c)
Isobaric Heat Capacity per Atom (r.u.)
3.896
3.893
3.890
3.887
Timestep (10^{-3} r.u.)
(d)
Isothermal Compressibility (r.u.)
0.2709
0.2705
0.2701
0.2697
0.2693
Timestep (10^{-3} r.u.)
(e)
Thermal expansion coefficient (r.u.)
0.3366
0.3360
0.3354
0.3348
Timestep (10^{-3} r.u.)
(f)

Figure S5. Comparison of the "middle-exp" decomposition with the "middle-sinh" decomposition for using the MTTK barostat in the MD simulations of liquid argon. The parameter of L-J potential is $= k_B \times 119.8\,\mathrm{K}$, $\sigma = 340.5\,\mathrm{pm}$ and $m = 39.962\,A_r$. The state point is chosen to be $\beta = 0.4\,\varepsilon$ and $P_{\mathrm{ext}} = 1.706\,\varepsilon/\sigma^3$. The calculated thermodynamic properties include (a) density, (b) enthalpy per atom, (c) isobaric heat capacity per atom, (d) isothermal compressibility and (e) thermal expansion coefficient. Black line: the "middle-exp" decomposition. Blue line: the "middle-sinh" decomposition (equivalent to the scheme **#5** in

Table S1). Sixty-four trajectories are equilibrated for 2.5×10^5 r.u. and then propagated for 2.5×10^5 r.u, , using a cubic box with periodic boundary conditions containing 256 particles. All data are divided into 16 groups to calculate the standard error. The friction parameter (γ_{Lang}) for the Langevin thermostat and (γ^V_{Lang}) for the barostat are 5.0 r.u. and 0.5 r.u., respectively. The "piston" mass W is set to 1000 r.u. A smooth cutoff is chosen, i.e., the potential is truncated at $r_c = 3.0\sigma$ and is shifted to zero from $r_s = 2.5\sigma$. For liquid argon, the reduced unit of time is 1.000×10^{-3} r.u. $= 1.000\times10^{-3}\sqrt{m\sigma^2/\varepsilon} = 2.1564$ fs. All MD simulations are performed by our independently developed MD/PIMD program. Note that the scale of the y-axis of each panel of Figure S5 is much smaller than that of the corresponding panel of Figure 4. Panel (f) is a snapshot of 256 Lennard-Jones particles in a cubic box with periodic boundary conditions.

S3. Derivation of the "Middle" Scheme with the SCR Barostat

Instead of the category of extended-system barostatting methods such as the MTTK barostat, we can use the category of weak coupling barostat.

One example is the Berendsen barostat[19]. In the Berendsen barostat, the internal pressure of the system and the external pressure satisfy the first-order response relation

$$\frac{\mathrm{d}P_{\mathrm{int}}}{\mathrm{d}t} = \frac{P_{\mathrm{ext}} - P_{\mathrm{int}}}{\tau_P}, \tag{S72}$$

where τ_P is the characteristic time of the barostat. However, it has been shown that, in many cases, the Berendsen barostat fails to properly reproduce the volume distribution of the isobaric-isothermal ensemble[20]. The Berendsen barostat should not be recommended.

Another example is the Stochastic Cell-Rescaling (SCR) barostat[21], which is constructed from the Berendsen barostat and correctly describes the volume fluctuation[21]. The equation of motion of the volume variable in the SCR barostat is

$$\mathrm{d}V = -\frac{\kappa_T V}{\tau_P}\left(P_{\mathrm{ext}} - P_{\mathrm{int}} - \frac{k_B T}{V}\right)\mathrm{d}t + \sqrt{\frac{2k_B T \kappa_T V}{\tau_P}}\mathrm{d}W_t, \tag{S73}$$

where W_t is the Wiener process. After using Ito's lemma and applying the Fokker-Planck equation to eq (S73), we obtain the Kolmogorov operators of the decomposition of the SCR barostat in the main text reads

$$\mathcal{L}_{\mathbf{x}}\rho = -\mathbf{p}^T\mathbf{M}^{-1}\frac{\partial\rho}{\partial\mathbf{x}} = \rho\left(\beta\mathbf{p}^T\mathbf{M}^{-1}\frac{\partial U}{\partial\mathbf{x}}\right), \tag{S74}$$

$$\mathcal{L}_{\mathbf{p}}\rho = \left(\frac{\partial U}{\partial\mathbf{x}}\right)^T\frac{\partial\rho}{\partial\mathbf{p}} = \rho\left(-\beta\mathbf{p}^T\mathbf{M}^{-1}\frac{\partial U}{\partial\mathbf{x}}\right), \tag{S75}$$

$$\mathcal{L}_T\rho = \gamma_{\mathrm{Lang}}\left(\frac{\partial}{\partial\mathbf{p}}\right)^T(\mathbf{p}\rho) + \frac{\gamma_{\mathrm{Lang}}}{\beta}\left(\frac{\partial}{\partial\mathbf{p}}\right)^T\mathbf{M}\frac{\partial\rho}{\partial\mathbf{p}} = 0, \tag{S76}$$

$$
\begin{aligned}
&\mathcal{L}_{Bar}^{\mathrm{MD}}\rho(V^{1/d}\mathbf{s},V^{-1/d}\boldsymbol{\pi},V)\\
&=\frac{\kappa_T}{\tau_P}\frac{\partial}{\partial V}\left[\left(P_{\mathrm{ext}}-P_{\mathrm{int}}-\frac{k_BT}{V}\right)V\rho+k_BT\frac{\partial}{\partial V}(V\rho)\right]\\
&=\frac{\kappa_T}{\tau_P}\frac{\partial}{\partial V}\left[-VP_{\mathrm{int}}\rho-V\left((V^{-1/d}\boldsymbol{\pi})^T\mathbf{M}^{-1}\left(-\frac{1}{d}\right)(V^{-1/d-1}\boldsymbol{\pi})+\left(\frac{\partial U}{\partial\mathbf{s}}\right)^T\left(\frac{1}{d}\right)(V^{1/d-1}\mathbf{s})\right)\rho\right] \quad . \quad \text{(S77)}\\
&=\frac{\kappa_T}{\tau_P}\frac{\partial}{\partial V}\left[-VP_{\mathrm{int}}\rho-V\left(-\frac{2K}{dV}+\frac{1}{dV}\left(\frac{\partial U}{\partial\mathbf{x}}\right)^T\mathbf{x}\right)\rho\right]=0
\end{aligned}
$$

where $\mathbf{s}=V^{-1/d}\mathbf{x}$ and $\boldsymbol{\pi}=V^{1/d}\mathbf{p}$ is the scaled coordinate and momentum[21, 22], corresponding to the phase space evolution operators eqs (31)-(32) of the main text. The distribution function $\rho(\mathbf{x},\mathbf{p},V,p_\varepsilon)$ of eq (S55) is substituted in the right-hand side of each of eqs (S74)-(S77). Equations (S74)-(S77) lead to

$$
\mathcal{L}_{SCR}^{(\mathrm{full})}\rho\equiv\left(\mathcal{L}_{\mathbf{x}}+\mathcal{L}_{\mathbf{p}}+\mathcal{L}_{Bar}^{\mathrm{MD}}+\mathcal{L}_T\right)\rho=0, \quad \text{(S78)}
$$

Equation (S73) can be recast into an equivalent equation with $\varepsilon=\ln(V/V_0)$, where V_0 is the unit volume,

$$
\mathrm{d}\varepsilon=-\frac{\kappa_T}{\tau_P}(P_{\mathrm{ext}}-P_{\mathrm{int}})\mathrm{d}t+\sqrt{\frac{2k_BT\kappa_T}{V\tau_P}}\mathrm{d}W_t \quad . \quad \text{(S79)}
$$

In ref [21], it is shown that the equations of motion of the SCR barostat can be viewed as the high-friction limit of those in the following form of the MTTK barostat:

$$
\dot{\mathbf{x}}=\mathbf{M}^{-1}\mathbf{p}+\frac{p_\varepsilon}{W}\mathbf{x} \quad , \quad \text{(S80)}
$$

$$
\dot{\mathbf{p}}=-\frac{\partial U}{\partial\mathbf{x}}-\frac{p_\varepsilon}{W}\mathbf{p}-\gamma_{\mathrm{Lang}}\mathbf{p}+\sqrt{\frac{2\gamma_{\mathrm{Lang}}}{\beta}}\mathbf{M}^{1/2}\boldsymbol{\zeta}(t) \quad , \quad \text{(S81)}
$$

$$
\dot{\varepsilon}=\frac{dp_\varepsilon}{W} \quad , \quad \text{(S82)}
$$

$$
\dot{p}_\varepsilon=dV\left(P_{\mathrm{int}}-P_{\mathrm{ext}}+\frac{k_BT}{V}\right)-\gamma_{\mathrm{Lang}}^V p_\varepsilon+\sqrt{\frac{2W\gamma_{\mathrm{Lang}}^V}{\beta}}\zeta_\varepsilon(t) \quad . \quad \text{(S83)}
$$

Equations (S80)-(S83) are directly obtained from eq (S54) by substituting the term $\frac{d}{N_f}\mathbf{p}^T\mathbf{M}^{-1}\mathbf{p}$ by dk_BT in its last equation. Equations (S82)-(S83) can be recast into a second-order differential equation:

$$W\ddot{\varepsilon} = d^2V(\tilde{P}_{\text{int}} - P_{\text{ext}}) - W\gamma^V_{\text{Lang}}\dot{\varepsilon} + d\sqrt{\frac{2W\gamma^V_{\text{Lang}}}{\beta}}\xi_\varepsilon(t) \quad . \tag{S84}$$

The high-friction limit of eq (S84) is[21, 23]

$$\mathrm{d}\varepsilon = \frac{d^2}{W\gamma^V_{\text{Lang}}}\left(V(\tilde{P}_{\text{int}} - P_{\text{ext}}) - \frac{1}{\beta}\frac{\mathrm{d}\ln\gamma^V_{\text{Lang}}}{\mathrm{d}\varepsilon}\right)\mathrm{d}t + \sqrt{\frac{2d^2}{\beta W\gamma^V_{\text{Lang}}}}\mathrm{d}W_t \quad . \tag{S85}$$

If we choose

$$W\gamma^V_{\text{Lang}} = \frac{d^2\tau_P V}{\kappa_T} \quad , \tag{S86}$$

the equations of the MTTK barostat then become those of the SCR barostat.

The SCR barostat requires rescaling of the coordinate of the particle and, sometimes, the velocity of the particle after each volume-updating step. In ref [21], three integrators for the SCR barostat are proposed, namely, "Euler," "Reversible," and "Trotter". Since the Euler integrator $e^{\mathcal{L}^{\text{Euler}}_{\text{NPT}}\Delta t} = e^{\mathcal{L}_T\Delta t/2}e^{\mathcal{L}^{\text{MD}}_{\text{Bar}}\Delta t}e^{\mathcal{L}_{\mathbf{p}}\Delta t/2}e^{\mathcal{L}_{\mathbf{x}}\Delta t}e^{\mathcal{L}_{\mathbf{p}}\Delta t/2}e^{\mathcal{L}_T\Delta t/2}$, which minimizes the computation of forces and virial terms in the evolution of a full time step Δt, is the most efficient among the three integrators of ref [21], we employ it for comparison. It is evident that the Euler integrator of ref [21] falls into the category of the conventional "side" scheme described in the main text. We then use "side SCR" to denote the Euler integrator of the SCR barostat of ref [21].

In the main text, we derive the "middle" scheme with the SCR barostat, e.g.,

$e^{\mathcal{L}_{\mathrm{NPT}}^{\mathrm{Middle}}\Delta t} = e^{\mathcal{L}_{\mathrm{Bar}}^{\mathrm{MD}}\Delta t} e^{\mathcal{L}_{\mathbf{x}}\Delta t/2} e^{\mathcal{L}_{T}\Delta t} e^{\mathcal{L}_{\mathbf{x}}\Delta t/2} e^{\mathcal{L}_{\mathbf{p}}\Delta t}$ based on the leap-frog algorithm. **Figure S6** shows the results for liquid water when MD simulations with the SCR barostat are performed. Figure S6 suggests that the "middle" scheme is superior to the conventional "side" scheme for the implementation of the SCR barostat. For instance, the density produced by the "middle" scheme with the SCR barostat exhibits an absolute deviation of only $3\times10^{-4}\ \mathrm{g\cdot cm^{-3}}$ at $\Delta t = 2.0$ fs from the converged values, while the corresponding deviation for the "side" scheme with the SCR barostat is $\sim 3.4\times10^{-2}\ \mathrm{g\cdot cm^{-3}}$. When other properties are tested, the recommended "middle" scheme also significantly outperforms the conventional "side" scheme for the implementation of the SCR barostat. Figure S6 also demonstrates that the performance of the "middle" scheme with the MTTK barostat is similar to that of the "middle" scheme with the SCR barostat. When the "middle" scheme is utilized, the MTTK barostat and the SCR barostat lead to almost the same results for the isobaric-isothermal ensemble.

The choice of parameter κ_T is, however, important for efficient simulations with the SCR barostat. The strategy for choosing the value of κ_T is discussed in the main text. However, when systems are under extreme conditions, e.g., high-pressure superfluid, where κ_T is often unknown, an unreasonable value of κ_T introduces errors for the NPT simulation. The relation of eq (S86) can be used to estimate the value of κ_T from some primitive calculation.

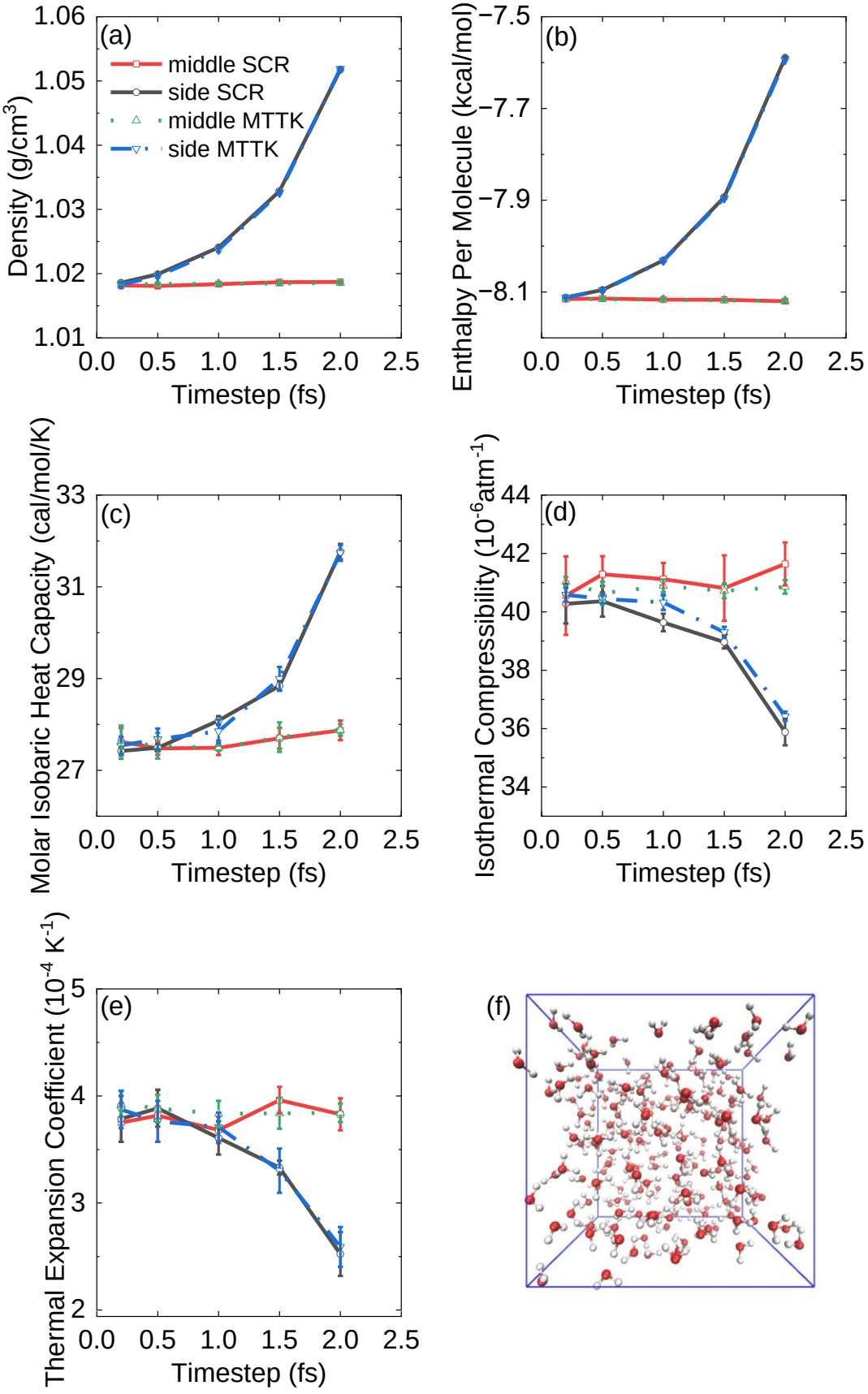
(a)
middle SCR
side SCR
middle MTTK
side MTTK
Density (g/cm3)
Timestep (fs)
(b)
Enthalpy Per Molecule (kcal/mol)
Timestep (fs)
(c)
Molar Isobaric Heat Capacity (cal/mol/K)
Timestep (fs)
(d)
Isothermal Compressibility (10-6atm-1)
Timestep (fs)
(e)
Thermal Expansion Coefficient (10-4 K-1)
Timestep (fs)
(f)

Figure S6. Results of NPT MD simulations for liquid water at $T = 298.15\,\mathrm{K}$ and $P_{\mathrm{ext}} = 1\,\mathrm{atm}$ using q-SPC/fw model with increasing time intervals. The SCR barostat is used for the simulation. Data of simulations with MTTK barostat is the same as **Figure 6** of the main text. The calculated thermodynamic properties include (a) density, (b) enthalpy per molecule, (d) molar isobaric heat capacity, (e) isothermal compressibility, and (f) thermal expansion coefficient. Red lines: the "middle" scheme with the SCR barostat, Black lines: the conventional "side" scheme with the SCR barostat. Green lines: the "middle" scheme with the MTTK barostat. Blue lines: the conventional "side" scheme with the MTTK barostat. 20 trajectories are equilibrated for 1 ns and propagated for 10 ns using a cubic box with periodic boundary conditions containing 216 molecules. All data are divided into 20 groups to calculate the standard error. The friction parameter (γ_{Lang}) for the Langevin thermostat is $5.0\,\mathrm{ps}^{-1}$. The characteristic time (τ_P) for the SCR barostat is $2.0\,\mathrm{ps}$ and the isothermal compressibility (κ_T) is $4.5\times10^{-5}\,\mathrm{bar}^{-1}$. The cutoff for the short-range interactions is 9 Å. All MD simulations are performed by our modified DL_POLY_2 package[14]. Panel (f) is a snapshot of 216 water molecules in a cubic box with periodic boundary conditions.

S4. "Middle" Scheme for the Isobaric-Isothermal Ensemble with Holonomic Constraints

Holonomic constraints are widely applied in molecular simulations of biological systems. By introducing holonomic constraints to high-frequency oscillatory degrees of freedom, it is possible to accelerate the simulation by significantly increasing the time interval. The "middle" scheme for canonical (constant-NVT) ensembles with holonomic constraints has already been developed in ref [13] and implemented in AMBER[24, 25] and other simulation packages. In this section, we extend our earlier work[13] to the "middle" scheme for the isobaric-isothermal ensembles

with holonomic constraints.

1) Atomic Pressure and Molecular Pressure

In the main text, the internal pressure estimator of eq (23), often referred to as the atomic pressure, assumes that all degrees of freedom, including high-frequency modes such as O-H stretches, are rescaled after each volume-updating step. This assumption is indicated in the non-linear term in the evolution of coordinates, e.g., in eqs (19)-(23) of the MTTK barostat in the main text.

In contrast, the molecular pressure can be constructed using the center of mass of the molecule[16, 18, 26-28], which is defined as

$$P_{\text{int,mol}} = \frac{1}{3V}\left(\sum_{I=1}^{N_m} \frac{\mathbf{P}_I^2}{M_I} + \sum_{I=1}^{N_m} \mathcal{F}_I \cdot \mathbf{R}_I \right) \quad , \tag{S87}$$

where $\mathbf{R}_I$ and $\mathbf{P}_I$ denote the coordinate and momentum vectors of the center of mass of the *I*-th molecule, respectively, $\mathcal{F}_I$ is the force acting on the center of mass of the *I*-th molecule, M_I represents the total mass of the *I*-th molecule, and N_m is the number of molecules. The equations of motion of the MTTK barostat using the molecular pressure are

$$\dot{\mathbf{x}}_{i,I} = \frac{\mathbf{p}_{i,I}}{m_{i,I}} + \frac{p}{W}\mathbf{R}_I \quad , \tag{S88}$$

$$\dot{\mathbf{p}}_{i,I} = -\frac{\partial U}{\partial \mathbf{x}_{i,I}} - \left(1 + \frac{1}{N_m}\right)\frac{p}{W}\frac{m_{i,I}}{M_I}\mathbf{P}_I \quad , \tag{S89}$$

$$\dot{V} = \frac{dVp_\varepsilon}{W} \quad , \tag{S90}$$

$$\dot{p}_\varepsilon = dV\left(P_{\text{int,mol}} - P_{\text{ext}}\right) + \frac{1}{N_m}\sum_{I=1}^{N_m}\frac{\mathbf{P}_I^2}{M_I} \quad , \tag{S91}$$

where $\mathbf{x}_{i,I}$, $\mathbf{p}_{i,I}$ and $m_{i,I}$ are the coordinate, momentum, and mass of the *i*-th atom of the *I*-th molecule, respectively. It is straightforward to use the Fokker-Planck equation to verify eqs (S88) -(S91) correctly reproduce the distribution function of the isobaric-isothermal ensemble.

Similarly, the equations of motion of the SCR barostat with the molecular pressure are

$$\dot{\mathbf{x}}_{i,I} = \frac{\mathbf{p}_{i,I}}{m_{i,I}} + \frac{\dot{V}}{dV}\mathbf{R}_i \quad , \tag{S92}$$

$$\dot{\mathbf{p}}_{i,I} = \mathbf{F}_{i,I} - \frac{\dot{V}}{dV}\frac{m_{i,I}}{M_I}\mathbf{P}_I \quad , \tag{S93}$$

$$\mathrm{d}V = V\frac{\kappa_T}{\tau_P}(P_{\mathrm{int,mol}} - P_{\mathrm{ext}})\mathrm{d}t + \sqrt{\frac{2\kappa_T V k_B T}{\tau_p}}\mathrm{d}W_t \quad . \tag{S94}$$

It is easy to prove that the distribution function of the isobaric-isothermal ensemble is stationary for eqs (S92)-(S94).

2) "Middle" Scheme for the Isobaric-Isothermal Ensemble with Holonomic Constraints

As shown by Kalibaeva *et al.* in ref [26] and by Martyna *el al* in ref [7], when performing MD simulations of the isothermal-isobaric ensemble for systems with holonomic constraints, the internal pressure can be estimated by using either the molecular virial expression or atomic virial expression. The molecular virial approach can be straightforwardly implemented with the application of the SHAKE[29] or RATTLE[30] algorithm. This is because intramolecular interactions and constraint processes (e.g., bond length/angle constraints) do not contribute to the internal pressure and do not respond to the pressure fluctuation. We implement the recommended "middle" scheme with holonomic constraints in AMBER/AmberTools where the molecular virial

expression is used.

The conventional "side" schemes as well as the "middle" scheme using the MTTK barostat with holonomic constraints and those using the SCR barostat with holonomic constraints are listed in **Table S3** and **Table S4** , respectively. As described in ref [13], the coordinate-constraining step C_1 and momentum-constraining step C_2 refer to the constraining procedures for the coordinate and momentum vectors in the RATTLE algorithm. When the system is subject to n_c holonomic constraints

$$\boldsymbol{\sigma}(\mathbf{x}) = 0 \quad , \tag{S95}$$

$$\frac{\mathrm{d}}{\mathrm{d}t}\boldsymbol{\sigma}(\mathbf{x}) = \left(\frac{\partial \boldsymbol{\sigma}}{\partial \mathbf{x}}\right)^T \mathbf{M}^{-1}\mathbf{p} = 0 \quad , \tag{S96}$$

where $\boldsymbol{\sigma}(\mathbf{x})$ is a vector with n_c dimensions, and the time derivative implies the constraint for the momentum vector. The coordinate-constraining step C_1 of the Rattle algorithm is

$$C_1 : \begin{cases} \text{solve}\,\boldsymbol{\lambda} : \boldsymbol{\sigma}\left(\tilde{\mathbf{x}}(\Delta t) + \mathbf{M}^{-1}\dfrac{\partial \boldsymbol{\sigma}}{\partial \mathbf{x}(0)}\boldsymbol{\lambda}\right) = 0 \\ \mathbf{x}(\Delta t) \leftarrow \tilde{\mathbf{x}}(\Delta t) + \mathbf{M}^{-1}\dfrac{\partial \boldsymbol{\sigma}}{\partial \mathbf{x}(0)}\boldsymbol{\lambda} \\ \mathbf{p}(\Delta t/2) \leftarrow \tilde{\mathbf{p}}(\Delta t/2) + \dfrac{1}{\Delta t}\dfrac{\partial \boldsymbol{\sigma}}{\partial \mathbf{x}(0)}\boldsymbol{\lambda} \end{cases} , \tag{S97}$$

where $\tilde{\mathbf{x}}(\Delta t)$ and $\tilde{\mathbf{p}}(\Delta t/2)$ are the coordinate and momentum vectors before the constraining step, and they do not satisfy the holonomic constraint conditions. In eq (S97), $\boldsymbol{\lambda}$ is the n_c-demensional vector of Lagrange multipliers. For triatomic molecules, such as the water molecule, holonomic constraints can be analytically solved by the SETTLE algorithm[31]. For general molecular systems, $\boldsymbol{\lambda}$ can be numerically solved in an iterative fashion using Newton's method,

of which the iteration step reads

$$\begin{aligned} &\text{solve}\,\bar{\boldsymbol{\lambda}}:\left(\frac{\partial\boldsymbol{\sigma}}{\partial\bar{\mathbf{x}}}\right)^{T}\mathbf{M}^{-1}\frac{\partial\boldsymbol{\sigma}}{\partial\mathbf{x}(0)}\bar{\boldsymbol{\lambda}}=-\boldsymbol{\sigma}(\bar{\mathbf{x}}) \\ &\bar{\mathbf{x}}\leftarrow\bar{\mathbf{x}}+\mathbf{M}^{-1}\frac{\partial\boldsymbol{\sigma}}{\partial\mathbf{x}(0)}\bar{\boldsymbol{\lambda}} \\ &\boldsymbol{\lambda}\leftarrow\boldsymbol{\lambda}+\bar{\boldsymbol{\lambda}} \end{aligned} \quad . \tag{S98}$$

where the initial values for $\bar{\mathbf{x}}$ and $\boldsymbol{\lambda}$ can be set as $\bar{\mathbf{x}}=\tilde{\mathbf{x}}(\Delta t)$ and $\boldsymbol{\lambda}=0$, respectively. When the number of constraints n_c is small, the vector $\bar{\boldsymbol{\lambda}}$ can be efficiently solved by LU decomposition, this approach is termed the m-SHAKE algorithm[32]. When the system involves a large number of constraints, the iteration can be performed to satisfy each holonomic constraint in succession, which is more numerically favorable[13].

The momentum-constraining step C_2 of the Rattle algorithm is

$$C_2:\begin{cases}\text{solve}\,\boldsymbol{\mu}:\left(\dfrac{\partial\boldsymbol{\sigma}}{\partial\mathbf{x}(\Delta t)}\right)^{T}\mathbf{M}^{-1}\left(\tilde{\mathbf{p}}(\Delta t)+\dfrac{\partial\boldsymbol{\sigma}}{\partial\mathbf{x}(\Delta t)}\boldsymbol{\mu}\right)=0 \\ \mathbf{p}(\Delta t)\leftarrow\tilde{\mathbf{p}}(\Delta t)+\dfrac{\partial\boldsymbol{\sigma}}{\partial\mathbf{x}(\Delta t)}\boldsymbol{\mu}\end{cases}, \tag{S99}$$

$\boldsymbol{\mu}$ is an n_c-demensional vector, which can also be solved by Newton's method

$$\text{solve}\,\boldsymbol{\mu}:\left(\frac{\partial\boldsymbol{\sigma}}{\partial\mathbf{x}(\Delta t)}\right)^{T}\mathbf{M}^{-1}\frac{\partial\boldsymbol{\sigma}}{\partial\mathbf{x}(\Delta t)}\boldsymbol{\mu}=-\left(\frac{\partial\boldsymbol{\sigma}}{\partial\mathbf{x}(\Delta t)}\right)^{T}\mathbf{M}^{-1}\tilde{\mathbf{p}}(\Delta t) \quad . \tag{S100}$$

The SETTLE algorithm can be employed to analytically solve the constraints for triatomic molecules. When the system involves a small number of constraints, vector $\boldsymbol{\mu}$ can be straightforwardly solved by the Cholesky decomposition. When the number of constraints is large, it is more reasonable to apply the iteration to each of holonomic constraints in succession as described in ref [13].

Table S3. The "Middle" Schemes with the MTTK Barostat and Holonomic Constraints

Scheme	Decomposition Order
Side	$B-T-p_V-C_2-p_r-p-V-C_2-C_1-x_r-x-p-p_r-p_V-T-B$
Middle	$p_V-V-C_2-C_1-x_r-B-x-T-x-B-x_r-V-p_V-C_2-p_r-p$

Table S4. The "Middle" Schemes with the SCR Barostat and Holonomic Constraints

Scheme	Decomposition Order
Side in GROMACS	$T-C_2-p-p_r-x_r-V-C_2-C_1-x-p-T$
Side in AMBER	$p_r-x_r-V-C_1-x-p-T$
Middle	$p_r-x_r-V-C_2-C_1-x-T-x-C_2-p$

We have implemented the "middle" scheme with the SCR barostat (with holonomic constraints), as described in **Table S4**, into AMBER and AmberTools[24, 25], where the molecular virial and molecular pressure are used. The MD simulations of liquid water with the SPC/E model, where intramolecular motion is fixed, are performed using the modified "pmemd" module of AMBER with CPU-based parallelization and with GPU-accelerated computing. Simulation results are shown in **Figure 8** in the main text. The time interval can also be as large as ~6 fs. When AMBER is used, the "middle" scheme outperforms the conventional "side" scheme in the calculation of thermodynamic properties (density, enthalpy, isobaric heat capacity, isothermal compressibility, and thermal expansion coefficient).

S5: Numerical Algorithms for the "Middle" Scheme.

In this section we present the details of the MD and PIMD algorithms of the recommended "middle" scheme. Below we use the velocity-Verlet-based version for demonstration. It is trivial to extend the algorithms to those of the leap-frog-based version.

1) "Middle" Scheme with the MTTK Barostat for MD

The velocity-Verlet-based algorithm for the "middle" scheme with the MTTK barostat for MD reads

$$e^{\mathcal{L}_{\mathbf{p}}\Delta t/2}:\mathbf{p}\leftarrow\mathbf{p}-\frac{\Delta t}{2}\frac{\partial U}{\partial \mathbf{x}},$$

$$e^{\mathcal{L}_{\mathbf{p}_r}\Delta t/2}:\mathbf{p}\leftarrow\mathbf{p}e^{-\left(1+\frac{d}{N_f}\right)\frac{p_\varepsilon}{W}\frac{\Delta t}{2}},$$

(Momentum-constraining step C_2 if holonomic constraints are requied)

$$e^{\mathcal{L}_{\mathbf{p}_\varepsilon}\Delta t/2}:p_\varepsilon\leftarrow p_\varepsilon+dV(P_{\text{int}}-P_{\text{ext}})\frac{\Delta t}{2}+\frac{d}{N_f}\mathbf{p}^T\mathbf{M}^{-1}\mathbf{p}\frac{\Delta t}{2},$$

$$e^{\mathcal{L}_V\Delta t/2}:V\leftarrow Ve^{d\frac{p_\varepsilon}{W}\frac{\Delta t}{2}},$$

$$e^{\mathcal{L}_{\mathbf{x}_r}\Delta t/2}:\mathbf{x}\leftarrow\mathbf{x}e^{\frac{p_\varepsilon}{W}\frac{\Delta t}{2}},$$

$$e^{\mathcal{L}_B\Delta t/2}:p_\varepsilon\leftarrow e^{-\gamma_{\text{Lang}}^V\Delta t/2}p_\varepsilon+\sqrt{1-e^{-\gamma_{\text{Lang}}^V\Delta t}}\sqrt{\frac{1}{\beta}}W^{1/2}\eta_\varepsilon(t),$$

$$e^{\mathcal{L}_{\mathbf{x}}\Delta t/2}:\mathbf{x}\leftarrow\mathbf{x}+\frac{\Delta t}{2}\mathbf{M}^{-1}\mathbf{p},$$

$$e^{\mathcal{L}_T\Delta t}:\mathbf{p}\leftarrow e^{-\gamma_{\text{Lang}}\Delta t}\mathbf{p}+\sqrt{1-e^{-2\gamma_{\text{Lang}}\Delta t}}\sqrt{\frac{1}{\beta}}\mathbf{M}^{1/2}\boldsymbol{\eta}(t),$$

$$e^{\mathcal{L}_{\mathbf{x}}\Delta t/2}:\mathbf{x}\leftarrow\mathbf{x}+\frac{\Delta t}{2}\mathbf{M}^{-1}\mathbf{p},$$

$$e^{\mathcal{L}_B\Delta t/2}:p_\varepsilon\leftarrow e^{-\gamma_{\text{Lang}}^V\Delta t/2}p_\varepsilon+\sqrt{1-e^{-\gamma_{\text{Lang}}^V\Delta t}}\sqrt{\frac{1}{\beta}}W^{1/2}\eta_\varepsilon(t+\Delta t/2),$$

$$e^{\mathcal{L}_{\mathbf{x}_r}\Delta t/2}:\mathbf{x}\leftarrow\mathbf{x}e^{\frac{p_\varepsilon}{W}\frac{\Delta t}{2}},$$

(Coordinate-constraining step C_1 and momentum-constraining step C_2 if holonomic constraints are requied)

$$e^{\mathcal{L}_V\Delta t/2}:V\leftarrow Ve^{d\frac{p_\varepsilon}{W}\frac{\Delta t}{2}},$$

(Force calculation)

$$e^{\mathcal{L}_{p_\varepsilon}\Delta t/2}:p_\varepsilon\leftarrow p_\varepsilon+dV(P_{\text{int}}-P_{\text{ext}})\frac{\Delta t}{2}+\frac{d}{N_f}\mathbf{p}^T\mathbf{M}^{-1}\mathbf{p}\frac{\Delta t}{2},$$

$$e^{\mathcal{L}_{\mathbf{p}_r}\Delta t/2}:\mathbf{p}\leftarrow\mathbf{p}e^{-\left(1+\frac{d}{N_f}\right)\frac{p_\varepsilon}{W}\frac{\Delta t}{2}},$$

$$e^{\mathcal{L}_{\mathbf{p}}\Delta t/2}:\mathbf{p}\leftarrow\mathbf{p}-\frac{\Delta t}{2}\frac{\partial U}{\partial \mathbf{x}},\tag{S101}$$

where $\eta_\varepsilon(t)$ is a gaussian standard random number at a fixed time t with zero mean $\langle\eta_\varepsilon(t)\rangle=0$ and unit deviation $\left\langle\left(\eta_\varepsilon(t)\right)^2\right\rangle=1$ for updating the "piston" momentum p_ε, $\boldsymbol{\eta}(t)$ is a gaussian

standard random number vector at a fixed time t with zero mean $\langle \boldsymbol{\eta}(t) \rangle = \mathbf{0}$ and diagonal deviation matrix $\langle \boldsymbol{\eta}(t)\boldsymbol{\eta}^T(t) \rangle = \mathbf{1}$ for updating the particle momentum $\mathbf{p}$, and $\eta_\varepsilon(t + \Delta t/2)$ is a gaussian standard random number at a fixed time $t + \Delta t/2$ with zero mean $\langle \eta_\varepsilon(t + \Delta t/2) \rangle = 0$ and unit deviation $\langle (\eta_\varepsilon(t + \Delta t/2))^2 \rangle = 1$ for updating the "piston" momentum p_ε. The coordinate-constraining step C_1 and momentum-constraining step C_2 of the RATTLE algorithm are defined in ref [13] and briefly described in Section S4 of the Supporting Information.

2) "Middle" Scheme with the MTTK Barostat for PIMD

The velocity-Verlet-based algorithm for the "middle" scheme with the MTTK barostat for PIMD using the "all-mode scaled" method for the internal pressure (eq (S13)) reads:

$$e^{\mathcal{L}_{\mathbf{p}}\Delta t/2}:\mathbf{p}_i \leftarrow \mathbf{p}_i - \frac{\Delta t}{2}\left(\frac{\partial \phi}{\partial \boldsymbol{\xi}_i} + \omega_P^2 \overline{\mathbf{M}}_i \boldsymbol{\xi}_i\right) \quad (i=1,\cdots,L),$$

$$e^{\mathcal{L}_{\mathbf{p}_r}\Delta t/2}:\mathbf{p}_i \leftarrow \mathbf{p}_i e^{-\left(1+\frac{d}{N_f L}\right)\frac{p_\varepsilon}{W}\frac{\Delta t}{2}} \quad (i=1,\cdots,L),$$

$$e^{\mathcal{L}_{p_\varepsilon}\Delta t/2}:p_\varepsilon \leftarrow p_\varepsilon + dV(P_{\text{int}}^{\text{PI,all-mode}} - P_{\text{ext}})\frac{\Delta t}{2} + \frac{d}{N_f L}\sum_{i=1}^{L}\mathbf{p}_i{}^T \mathbf{M}_i^{-1}\mathbf{p}_i \frac{\Delta t}{2},$$

$$e^{\mathcal{L}_V \Delta t/2}:V \leftarrow Ve^{d\frac{p_\varepsilon}{W}\frac{\Delta t}{2}},$$

$$e^{\mathcal{L}_{\mathbf{x}_r}\Delta t/2}:\boldsymbol{\xi}_i \leftarrow \boldsymbol{\xi}_i e^{\frac{p_\varepsilon}{W}\frac{\Delta t}{2}} \quad (i=1,\cdots,L),$$

$$e^{\mathcal{L}_B \Delta t/2}:p_\varepsilon \leftarrow e^{-\gamma_{\text{Lang}}^V \Delta t/2}p_\varepsilon + \sqrt{1-e^{-\gamma_{\text{Lang}}^V \Delta t}}\sqrt{\frac{1}{\beta}}W^{1/2}\eta_\varepsilon(t),$$

$$e^{\mathcal{L}_{\mathbf{x}}\Delta t/2}:\boldsymbol{\xi}_i \leftarrow \boldsymbol{\xi}_i + \frac{\Delta t}{2}\mathbf{M}_i^{-1}\mathbf{p}_i \quad (i=1,\cdots,L),$$

$$e^{\mathcal{L}_T \Delta t}:\mathbf{p}_i \leftarrow e^{-\gamma_{\text{Lang}}^{(i)}\Delta t}\mathbf{p} + \sqrt{1-e^{-2\gamma_{\text{Lang}}^{(i)}\Delta t}}\sqrt{\frac{1}{\beta}}\mathbf{M}_i^{1/2}\boldsymbol{\eta}(t) \quad (i=1,\cdots,L),$$

$$e^{\mathcal{L}_{\mathbf{x}}\Delta t/2}:\boldsymbol{\xi}_i \leftarrow \boldsymbol{\xi}_i + \frac{\Delta t}{2}\mathbf{M}_i^{-1}\mathbf{p}_i \quad (i=1,\cdots,L),$$

$$e^{\mathcal{L}_B \Delta t/2}:p_\varepsilon \leftarrow e^{-\gamma_{\text{Lang}}^V \Delta t/2}p_\varepsilon + \sqrt{1-e^{-\gamma_{\text{Lang}}^V \Delta t}}\sqrt{\frac{1}{\beta}}W^{1/2}\eta_\varepsilon(t+\Delta t/2),$$

$$e^{\mathcal{L}_{\mathbf{x}_r}\Delta t/2}:\boldsymbol{\xi}_i \leftarrow \boldsymbol{\xi}_i e^{\frac{p_\varepsilon}{W}\frac{\Delta t}{2}} \quad (i=1,\cdots,L),$$

$$e^{\mathcal{L}_V \Delta t/2}:V \leftarrow Ve^{d\frac{p_\varepsilon}{W}\frac{\Delta t}{2}},$$

(Force calculation)

$$e^{\mathcal{L}_{p_\varepsilon}\Delta t/2}:p_\varepsilon \leftarrow p_\varepsilon + dV(P_{\text{int}}^{\text{PI,all-mode}} - P_{\text{ext}})\frac{\Delta t}{2} + \frac{d}{N_f L}\sum_{i=1}^{L}\mathbf{p}_i{}^T \mathbf{M}_i^{-1}\mathbf{p}_i \frac{\Delta t}{2},$$

$$e^{\mathcal{L}_{\mathbf{p}_r}\Delta t/2}:\mathbf{p}_i \leftarrow \mathbf{p}_i e^{-\left(1+\frac{d}{N_f L}\right)\frac{p_\varepsilon}{W}\frac{\Delta t}{2}} \quad (i=1,\cdots,L),$$

$$e^{\mathcal{L}_{\mathbf{p}}\Delta t/2}:\mathbf{p}_i \leftarrow \mathbf{p}_i - \frac{\Delta t}{2}\left(\frac{\partial \phi}{\partial \boldsymbol{\xi}_i} + \omega_P^2 \overline{\mathbf{M}}_i \boldsymbol{\xi}_i\right) \quad (i=1,\cdots,L). \tag{S102}$$

Below we also present the velocity-Verlet-based algorithm for the "middle" scheme with the MTTK barostat for PIMD using the "reduced dynamics" method for the internal pressure (eq (S15)):

$$
\begin{aligned}
&e^{\mathcal{L}_{\mathbf{p}}\Delta t/2}:\mathbf{p}_i \leftarrow \mathbf{p}_i - \frac{\Delta t}{2}\left(\frac{\partial \phi}{\partial \boldsymbol{\xi}_i} + \omega_P^2 \overline{\mathbf{M}}_i \boldsymbol{\xi}_i\right) \quad (i=1,\cdots,L),\\
&e^{\mathcal{L}_{\mathbf{p}_r}\Delta t/2}:\mathbf{p}_1 \leftarrow \mathbf{p}_1 e^{-\left(1+\frac{d}{N_f}\right)\frac{p_\varepsilon}{W}\frac{\Delta t}{2}}\\
&e^{\mathcal{L}_{p_\varepsilon}\Delta t/2}: p_\varepsilon \leftarrow p_\varepsilon + dV(P_{\text{int}}^{\text{PI,reduced}} - P_{\text{ext}})\frac{\Delta t}{2} + \frac{d}{N_f}\mathbf{p}_1^{\,T}\mathbf{M}_1^{-1}\mathbf{p}_1\frac{\Delta t}{2},\\
&e^{\mathcal{L}_V\Delta t/2}: V \leftarrow V e^{d\frac{p_\varepsilon}{W}\frac{\Delta t}{2}},\\
&e^{\mathcal{L}_{\mathbf{x}_r}\Delta t/2}:\boldsymbol{\xi}_1 \leftarrow \boldsymbol{\xi}_1 e^{\frac{p_\varepsilon}{W}\frac{\Delta t}{2}}\\
&e^{\mathcal{L}_B\Delta t/2}: p_\varepsilon \leftarrow e^{-\gamma_{\text{Lang}}^V \Delta t/2} p_\varepsilon + \sqrt{1-e^{-\gamma_{\text{Lang}}^V\Delta t}}\sqrt{\frac{1}{\beta}}W^{1/2}\eta_\varepsilon(t),\\
&e^{\mathcal{L}_{\mathbf{x}}\Delta t/2}:\boldsymbol{\xi}_i \leftarrow \boldsymbol{\xi}_i + \frac{\Delta t}{2}\mathbf{M}_i^{-1}\mathbf{p}_i \quad (i=1,\cdots,L),\\
&e^{\mathcal{L}_T\Delta t}:\mathbf{p}_i \leftarrow e^{-\gamma_{\text{Lang}}^{(i)}\Delta t}\mathbf{p} + \sqrt{1-e^{-2\gamma_{\text{Lang}}^{(i)}\Delta t}}\sqrt{\frac{1}{\beta}}\mathbf{M}_i^{1/2}\boldsymbol{\eta}(t) \quad (i=1,\cdots,L),\\
&e^{\mathcal{L}_{\mathbf{x}}\Delta t/2}:\boldsymbol{\xi}_i \leftarrow \boldsymbol{\xi}_i + \frac{\Delta t}{2}\mathbf{M}_i^{-1}\mathbf{p}_i \quad (i=1,\cdots,L),\\
&e^{\mathcal{L}_{p_\varepsilon}\Delta t/2}: p_\varepsilon \leftarrow e^{-\gamma_{\text{Lang}}^V \Delta t/2} p_\varepsilon + \sqrt{1-e^{-\gamma_{\text{Lang}}^V\Delta t}}\sqrt{\frac{1}{\beta}}W^{1/2}\eta_\varepsilon(t+\Delta t/2),\\
&e^{\mathcal{L}_{\mathbf{x}_r}\Delta t/2}:\boldsymbol{\xi}_1 \leftarrow \boldsymbol{\xi}_1 e^{\frac{p_\varepsilon}{W}\frac{\Delta t}{2}}\\
&e^{\mathcal{L}_V\Delta t/2}: V \leftarrow V e^{d\frac{p_\varepsilon}{W}\frac{\Delta t}{2}},\\
&\quad \text{(Force calculation)}\\
&e^{\mathcal{L}_{p_\varepsilon}\Delta t/2}: p_\varepsilon \leftarrow p_\varepsilon + dV(P_{\text{int}}^{\text{PI,reduced}} - P_{\text{ext}})\frac{\Delta t}{2} + \frac{d}{N_f}\sum_{i=1}^{L}\mathbf{p}_1^{\,T}\mathbf{M}_1^{-1}\mathbf{p}_1\frac{\Delta t}{2},\\
&e^{\mathcal{L}_{\mathbf{p}_r}\Delta t/2}:\mathbf{p}_1 \leftarrow \mathbf{p}_1 e^{-\left(1+\frac{d}{N_f}\right)\frac{p_\varepsilon}{W}\frac{\Delta t}{2}}\\
&e^{\mathcal{L}_{\mathbf{p}}\Delta t/2}:\mathbf{p}_i \leftarrow \mathbf{p}_i - \frac{\Delta t}{2}\left(\frac{\partial \phi}{\partial \boldsymbol{\xi}_i} + \omega_P^2 \overline{\mathbf{M}}_i \boldsymbol{\xi}_i\right) \quad (i=1,\cdots,L).
\end{aligned}
\tag{S103}
$$

3) "Middle" Scheme with the SCR Barostat for MD

The velocity-Verlet-based algorithm for the "middle" scheme with the SCR barostat for MD is:

$$
\begin{aligned}
&e^{\mathcal{L}_{\mathbf{p}}\Delta t/2}: \mathbf{p} \leftarrow \mathbf{p} - \frac{\Delta t}{2}\frac{\partial U}{\partial \mathbf{x}},\\
&\quad \text{(Momentum-constraining step } C_2 \text{ if holonomic constraints are requied)}\\
&e^{\mathcal{L}_{\mathbf{x}}\Delta t/2}: \mathbf{x} \leftarrow \mathbf{x} + \frac{\Delta t}{2}\mathbf{M}^{-1}\mathbf{p},\\
&e^{\mathcal{L}_{T}\Delta t}: \mathbf{p} \leftarrow e^{-\gamma_{\text{Lang}}\Delta t}\mathbf{p} + \sqrt{1-e^{-2\gamma_{\text{Lang}}\Delta t}}\sqrt{\frac{1}{\beta}}M^{1/2}\boldsymbol{\eta}(t),\\
&e^{\mathcal{L}_{\mathbf{x}}\Delta t/2}: \mathbf{x} \leftarrow \mathbf{x} + \frac{\Delta t}{2}\mathbf{M}^{-1}\mathbf{p},\\
&\quad \text{(Coordinate-constraining step } C_1 \text{ and momentum-constraining step } C_2\\
&\quad \text{if holonomic constraints are requied)}\\
&\quad \text{(Force calculation)}\\
&e^{\mathcal{L}_{\varepsilon}\Delta t}: \varepsilon \leftarrow \varepsilon + \Delta\varepsilon,\\
&e^{\mathcal{L}_{\mathbf{x}_r}\Delta t}: \mathbf{x} \leftarrow \mathbf{x}e^{\Delta\varepsilon/d},\\
&e^{\mathcal{L}_{\mathbf{p}_r}\Delta t}: \mathbf{p} \leftarrow \mathbf{p}e^{-\Delta\varepsilon/d}.\\
&e^{\mathcal{L}_{\mathbf{p}}\Delta t/2}: \mathbf{p} \leftarrow \mathbf{p} - \frac{\Delta t}{2}\frac{\partial U}{\partial \mathbf{x}},
\end{aligned}
\tag{S104}
$$

where $\Delta\varepsilon$ is defined by eq (30) of the main text.

Similarly, we can readily construct the PIMD algorithm for the "middle" scheme with the SCR barostat.

S6. "Middle" Scheme in the Isobaric-Isothermal Ensemble for Anisotropic Systems

In the main text, we focus on the isobaric-isothermal (constant-NPT) ensemble for isotropic systems. When anisotropic systems like crystals are investigated, it is essential to account for changes in the shape of the simulation cell with periodic boundary conditions. In this section, we

extend the recommended "middle" scheme for studying anisotropic systems, where the volume fluctuation is anisotropic.

The partition function of the isobaric-isothermal (constant-NPT) ensemble for anisotropic systems is

$$\begin{aligned} Z_{\mathrm{NPT}} &= \frac{I_{\mathrm{N}}}{V_0}\int_0^\infty \mathrm{d}V \int \mathrm{d}\mathbf{h}_0 e^{-\beta P_{\mathrm{ext}} V} Z_{\mathrm{NVT}}(N,V,\mathbf{h}_0,T)\delta(\det(\mathbf{h}_0)-1) \\ &= \frac{I_{\mathrm{N}}}{V_0}\int_0^\infty \mathrm{d}V \int \mathrm{d}\mathbf{h} V^{1-d} e^{-\beta P_{\mathrm{ext}} V} Z_{\mathrm{NVT}}(N,V,\mathbf{h}_0,T)\delta(\det(\mathbf{h})-V), \end{aligned} \tag{S105}$$

where $\mathbf{h}=\{\mathbf{a},\mathbf{b},\mathbf{c}\}$ is the simulation cell matrix[16] and $\mathbf{h}_0 = V^{-1/3}\mathbf{h}$ is the unit cell matrix. With loss of generality, we consider the molecular system in the 3-dimensional space. The MTTK barostat for anisotropic systems is defined as [2, 33-36]

$$\dot{\mathbf{x}}_i = \frac{\mathbf{p}_i}{m_i} + \frac{\mathbf{p}_g}{W_g}\mathbf{x}_i, \tag{S106}$$

$$\dot{\mathbf{p}}_i = -\frac{\partial U}{\partial \mathbf{x}_i} - \frac{\mathbf{p}_g}{W_g}\mathbf{p}_i - \frac{1}{N_f}\frac{\mathrm{Tr}[\mathbf{p}_g]}{W_g}\mathbf{p}_i - \gamma_{\mathrm{Lang}}\mathbf{p}_i + \sqrt{\frac{2\gamma_{\mathrm{Lang}}}{\beta}}\mathbf{M}_i^{1/2}\boldsymbol{\eta}_i, \tag{S107}$$

$$\dot{\mathbf{h}} = \frac{\mathbf{p}_g \mathbf{h}}{W_g}, \tag{S108}$$

$$\dot{\mathbf{p}}_g = \det(\mathbf{h})(\mathbf{P}^{(\mathrm{int})} - \mathbf{I}P_{\mathrm{ext}}) + \frac{1}{N_f}\sum_i \frac{\mathbf{p}_i^2}{m_i}\mathbf{I} - \gamma_{\mathrm{Lang}}^V \mathbf{p}_g + \sqrt{\frac{2\gamma_{\mathrm{Lang}}^V}{\beta}} W_g^{1/2}\boldsymbol{\eta}_g, \tag{S109}$$

where $\mathbf{x}_i, \mathbf{p}_i$ are 3-dimensional coordinate and momentum vectors of the *i*-th particle or atom, $\mathbf{p}_g$ is a 3x3 matrix, and the internal pressure tensor $\mathbf{P}^{(\mathrm{int})}$ is defined as

$$P_{\alpha\beta}^{(\mathrm{int})} = \frac{1}{\det(\mathbf{h})}\sum_{i=1}^{N}\left[\frac{(\mathbf{p}_i{}^T\hat{\mathbf{e}}_\alpha)(\mathbf{p}_i{}^T\hat{\mathbf{e}}_\beta)}{m_i} + (\mathbf{F}_i{}^T\hat{\mathbf{e}}_\alpha)(\mathbf{x}_i{}^T\hat{\mathbf{e}}_\beta)\right]. \tag{S110}$$

Equations (S106)-(S109) lead to the stationary distribution of the isobaric-isothermal ensemble

$$\rho(\mathbf{x},\mathbf{p},\mathbf{h},\mathbf{p}_g) \propto \exp\left[-\beta\left(\frac{1}{2}\mathbf{p}^{\mathrm{T}}\mathbf{M}^{-1}\mathbf{p}+U(\mathbf{x})+P_{\mathrm{ext}}\det[\mathbf{h}]+\frac{\mathrm{Tr}[\mathbf{p}_g\mathbf{p}_g^{\mathrm{T}}]}{2W_g}\right)\right]\det[\mathbf{h}]^{1-d}. \quad \text{(S111)}$$

The corresponding Kolmogorov operators of eqs (S106)-(S109) and their operations on the density distribution function of eq (S111) are

$$\mathcal{L}_{\mathbf{x}}\rho=\sum_i\left[-\left(\frac{\mathbf{p}_i}{m_i}\right)^T\frac{\partial\rho}{\partial\mathbf{x}_i}\right]=\beta\rho\left(\sum_{i=1}^N\left(\frac{\mathbf{p}_i}{m_i}\right)^T\frac{\partial U}{\partial\mathbf{x}_i}\right), \quad \text{(S112)}$$

$$\mathcal{L}_{\mathbf{p}}\rho=\sum_i\left[\left(\frac{\partial U}{\partial\mathbf{x}_i}\right)^T\frac{\partial\rho}{\partial\mathbf{p}_i}\right]=-\beta\rho\left(\sum_{i=1}^N\left(\frac{\mathbf{p}_i}{m_i}\right)^T\frac{\partial U}{\partial\mathbf{x}_i}\right), \quad \text{(S113)}$$

$$\mathcal{L}_{\mathbf{x}_r}\rho=\sum_i\left[-\left(\frac{\partial}{\partial\mathbf{x}_i}\right)^T\left(\frac{\mathbf{p}_g}{W_g}\mathbf{x}_i\rho\right)\right]=-\frac{\rho}{W_g}\sum_{i=1}^N\left[\mathrm{Tr}[p_g]-\beta\left(\frac{\partial U}{\partial\mathbf{x}_i}\right)^T\mathbf{p}_g\mathbf{x}_i\right], \quad \text{(S114)}$$

$$\begin{aligned}\mathcal{L}_{\mathbf{p}_r}\rho&=\sum_i\left[\left(\frac{\partial}{\partial\mathbf{p}_i}\right)^T\left(\frac{\mathbf{p}_g}{W_g}\mathbf{p}_i\rho\right)+\frac{1}{N_f}\frac{\mathrm{Tr}[\mathbf{p}_g]}{W_g}\left(\frac{\partial}{\partial\mathbf{p}_i}\right)^T(\mathbf{p}_i\rho)\right]\\&=\frac{\rho}{W_g}\left[\sum_{i=1}^N\left(\mathrm{Tr}[\mathbf{p}_g]-\frac{\beta}{m_i}\mathbf{p}_i^T\mathbf{p}_g\mathbf{p}_i\right)+\mathrm{Tr}[\mathbf{p}_g]-\frac{\beta\,\mathrm{Tr}[\mathbf{p}_g]}{N_f}\sum_{i=1}^N\frac{\mathbf{p}_i^2}{m_i}\right],\end{aligned} \quad \text{(S115)}$$

$$\mathcal{L}_{\mathbf{h}}\rho=-\sum_{\alpha,\beta}\frac{\partial}{\partial h_{\alpha\beta}}\left(\frac{\mathbf{p}_g}{W_g}\mathbf{h}\rho\right)_{\alpha\beta}=\frac{\rho\,\mathrm{Tr}[\mathbf{p}_g]}{W_g}\left(\beta P_{\mathrm{ext}}\det[\mathbf{h}]-1\right), \quad \text{(S116)}$$

$$\begin{aligned}\mathcal{L}_{\mathbf{p}_g}\rho&=\sum_{\alpha,\beta}-\left(\det[\mathbf{h}]\left(P_{\alpha\beta}^{(\mathrm{int})}-P_{\mathrm{ext}}\delta_{\alpha\beta}\right)+\frac{1}{N_f}\sum_i\frac{\mathbf{p}_i^2}{m_i}\delta_{\alpha\beta}\right)\frac{\partial\rho}{\partial p_{g\alpha\beta}}\\&=\frac{\beta\rho}{W_g}\left[\sum_{i=1}^N\left(\frac{1}{m_i}\mathbf{p}_i^T\mathbf{p}_g\mathbf{p}_i-\left(\frac{\partial U}{\partial\mathbf{x}_i}\right)^T\mathbf{p}_g\mathbf{x}_i\right)-P_{\mathrm{ext}}\det[\mathbf{h}]\mathrm{Tr}[\mathbf{p}_g]+\frac{\mathrm{Tr}[\mathbf{p}_g]}{N_f}\sum_{i=1}^N\frac{\mathbf{p}_i^2}{m_i}\right],\end{aligned} \quad \text{(S117)}$$

$$\mathcal{L}_T\rho=\sum_i\left[\gamma_{\mathrm{Lang}}\left(\frac{\partial}{\partial\mathbf{p}_i}\right)^T(\mathbf{p}_i\rho)+\frac{\gamma_{\mathrm{Lang}}}{\beta}m_i\frac{\partial^2\rho}{\partial\mathbf{p}_i^2}\right]=0, \quad \text{(S118)}$$

$$\mathcal{L}_B\rho=\sum_{\alpha,\beta}\gamma_{\mathrm{Lang}}^V\frac{\partial}{\partial p_{g\alpha\beta}}(p_{g\alpha\beta}\rho)+\frac{\gamma_{\mathrm{Lang}}^V W_g}{\beta}\frac{\partial^2\rho}{\partial p_{g\alpha\beta}^2}=0. \quad \text{(S119)}$$

In the derivation of $\mathcal{L}_{\mathbf{h}}\rho$ of eq (S116), we use the identity:

$$\sum_{\beta=1}^{d} h_{\gamma\beta} \frac{\partial \det[\mathbf{h}]}{\partial h_{\alpha\beta}} = \delta_{\alpha\gamma} \det[\mathbf{h}] \tag{S120}$$

Equations (S112)-(S119) lead to

$$\mathcal{L}_{\mathrm{MTTK}}^{(\mathrm{full,aniso})} \rho \equiv \left(\mathcal{L}_{\mathbf{x}} + \mathcal{L}_{\mathbf{x}_r} + \mathcal{L}_{\mathbf{p}} + \mathcal{L}_{\mathbf{p}_r} + \mathcal{L}_{\mathbf{h}} + \mathcal{L}_{\mathbf{p}_g} + \mathcal{L}_T + \mathcal{L}_B \right) \rho = 0 \quad , \tag{S121}$$

i.e., $\rho(\mathbf{x}, \mathbf{p}, \mathbf{h}, \mathbf{p}_g)$ of eq (S111) is the stationary distribution of the anisotropic MTTK equation defined by eqs (S106)-(S109).

In the anisotropic case, the scalar internal pressure is replaced by the corresponding tensor form. Except this change, the performance of molecular dynamics is similar. The velocity-Verlet-based "middle" scheme

$$e^{\mathcal{L}_{\mathbf{p}} \Delta t/2} e^{\mathcal{L}_{\mathrm{Bar}(2)}^{\mathrm{MD}} \Delta t/2} e^{\mathcal{L}_{\mathbf{x}} \Delta t/2} e^{\mathcal{L}_T \Delta t} e^{\mathcal{L}_{\mathbf{x}} \Delta t/2} e^{\mathcal{L}_{\mathrm{Bar}(1)}^{\mathrm{MD}} \Delta t/2} e^{\mathcal{L}_{\mathbf{p}} \Delta t/2} \quad , \tag{S122}$$

as well as the leap-frog-based version

$$e^{\mathcal{L}_{\mathrm{Bar}(2)}^{\mathrm{MD}} \Delta t/2} e^{\mathcal{L}_{\mathbf{x}} \Delta t/2} e^{\mathcal{L}_T \Delta t} e^{\mathcal{L}_{\mathbf{x}} \Delta t/2} e^{\mathcal{L}_{\mathrm{Bar}(1)}^{\mathrm{MD}} \Delta t/2} e^{\mathcal{L}_{\mathbf{p}} \Delta t} \tag{S123}$$

is also recommended for the MTTK barostat for MD/PIMD simulations for the isobaric-isothermal ensemble for isotropic systems. In eq (S122) or eq (S123), $e^{\mathcal{L}_{\mathrm{Bar}(1)}^{\mathrm{MD}} \Delta t/2}$ and $e^{\mathcal{L}_{\mathrm{Bar}(2)}^{\mathrm{MD}} \Delta t/2}$ are defined by

$$e^{\mathcal{L}_{\mathrm{Bar}(1)}^{\mathrm{MD}} \Delta t} = e^{\mathcal{L}_B \Delta t} e^{\mathcal{L}_{\mathbf{x}_r} \Delta t} e^{\mathcal{L}_{\mathbf{h}} \Delta t} e^{\mathcal{L}_{\mathbf{p}_g} \Delta t} e^{\mathcal{L}_{\mathbf{p}_r} \Delta t} \tag{S124}$$

$$e^{\mathcal{L}_{\mathrm{Bar}(2)}^{\mathrm{MD}} \Delta t} = e^{\mathcal{L}_{\mathbf{p}_r} \Delta t} e^{\mathcal{L}_{p_\varepsilon} \Delta t} e^{\mathcal{L}_{\mathbf{p}_g} \Delta t} e^{\mathcal{L}_{\mathbf{h}} \Delta t} e^{\mathcal{L}_B \Delta t} \tag{S125}$$

The MD algorithm based on the velocity-Verlet algorithm for the "middle" scheme with anisotropic MTTK barostat is

$$
\begin{aligned}
&e^{\mathcal{L}_{\mathbf{p}}\Delta t/2}:\mathbf{p}_i \leftarrow \mathbf{p}_i - \frac{\Delta t}{2}\frac{\partial U}{\partial \mathbf{x}_i} \quad (i=1,\cdots,N_{\text{atom}}),\\
&e^{\mathcal{L}_{\mathbf{p}_r}\Delta t/2}:\mathbf{p}_i \leftarrow \exp\left(-\left(\frac{\mathbf{p}_g}{W_g}+\frac{1}{N}\frac{\mathrm{Tr}\left[\mathbf{p}_g\right]}{3W_g}\mathbf{I}\right)\frac{\Delta t}{2}\right)\mathbf{p}_i \quad (i=1,\cdots,N_{\text{atom}}),\\
&e^{\mathcal{L}_{\mathbf{p}_g}\Delta t/2}:\mathbf{p}_g \leftarrow \mathbf{p}_g + \det(\mathbf{h})\left(\mathbf{P}_{\text{int}}-\mathbf{I}P_{\text{ext}}\right)\frac{\Delta t}{2}+\frac{1}{3N}\sum_i^N\frac{\mathbf{p}_i^2}{m_i}\frac{\Delta t}{2},\\
&e^{\mathcal{L}_{\mathbf{h}}\Delta t/2}:\mathbf{h} \leftarrow \exp\left(\frac{\mathbf{p}_g}{W_g}\frac{\Delta t}{2}\right)\mathbf{h},\\
&e^{\mathcal{L}_{\mathbf{x}_r}\Delta t/2}:\mathbf{x}_i \leftarrow \exp\left(\frac{\mathbf{p}_g}{W_g}\frac{\Delta t}{2}\right)\mathbf{x}_i \quad (i=1,\cdots,N_{\text{atom}}),\\
&e^{\mathcal{L}_B\Delta t/2}:\mathbf{p}_g \leftarrow e^{-\gamma_{\text{Lang}}^V\Delta t/2}\mathbf{p}_g+\sqrt{1-e^{-\gamma_{\text{Lang}}^V\Delta t}}\sqrt{\frac{1}{\beta}}W_g^{1/2}\boldsymbol{\eta}^{(g)}(t),\\
&e^{\mathcal{L}_{\mathbf{x}}\Delta t/2}:\mathbf{x}_i \leftarrow \mathbf{x}_i+\frac{\Delta t}{2}\frac{1}{m_i}\mathbf{p}_i \quad (i=1,\cdots,N_{\text{atom}}),\\
&e^{\mathcal{L}_T\Delta t}:\mathbf{p}_i \leftarrow e^{-\gamma_{\text{Lang}}\Delta t}\mathbf{p}_i+\sqrt{1-e^{-2\gamma_{\text{Lang}}\Delta t}}\sqrt{\frac{m_i}{\beta}}\boldsymbol{\eta}_i(t) \quad (i=1,\cdots,N_{\text{atom}}),\\
&e^{\mathcal{L}_{\mathbf{x}}\Delta t/2}:\mathbf{x}_i \leftarrow \mathbf{x}_i+\frac{\Delta t}{2}\frac{1}{m_i}\mathbf{p}_i \quad (i=1,\cdots,N_{\text{atom}}),\\
&e^{\mathcal{L}_B\Delta t/2}:\mathbf{p}_g \leftarrow e^{-\gamma_{\text{Lang}}^V\Delta t/2}\mathbf{p}_g+\sqrt{1-e^{-\gamma_{\text{Lang}}^V\Delta t}}\sqrt{\frac{1}{\beta}}W_g^{1/2}\boldsymbol{\eta}^{(g)}(t+\Delta t/2),\\
&e^{\mathcal{L}_{\mathbf{x}}\Delta t/2}:\mathbf{x}_i \leftarrow \exp\left(\frac{\mathbf{p}_g}{W_g}\frac{\Delta t}{2}\right)\mathbf{x}_i \quad (i=1,\cdots,N_{\text{atom}}),\\
&e^{\mathcal{L}_{\mathbf{h}}\Delta t/2}:\mathbf{h} \leftarrow \exp\left(\frac{\mathbf{p}_g}{W_g}\frac{\Delta t}{2}\right)\mathbf{h},\\
&\quad\text{(Force calculation)}\\
&e^{\mathcal{L}_{\mathbf{p}_g}\Delta t/2}:\mathbf{p}_g \leftarrow \mathbf{p}_g + \det(\mathbf{h})\left(\mathbf{P}_{\text{int}}-\mathbf{I}P_{\text{ext}}\right)\frac{\Delta t}{2}+\frac{1}{3N}\sum_i^N\frac{\mathbf{p}_i^2}{m_i}\frac{\Delta t}{2},\\
&e^{\mathcal{L}_{\mathbf{p}_r}\Delta t/2}:\mathbf{p}_i \leftarrow \exp\left(-\left(\frac{\mathbf{p}_g}{W_g}+\frac{1}{N}\frac{\mathrm{Tr}\left[\mathbf{p}_g\right]}{3W_g}\mathbf{I}\right)\frac{\Delta t}{2}\right)\mathbf{p}_i \quad (i=1,\cdots,N_{\text{atom}}),\\
&e^{\mathcal{L}_{\mathbf{p}}\Delta t/2}:\mathbf{p}_i \leftarrow \mathbf{p}_i - \frac{\Delta t}{2}\frac{\partial U}{\partial \mathbf{x}_i} \quad (i=1,\cdots,N_{\text{atom}}),
\end{aligned}
\tag{S126}
$$

where $\exp(\cdot)$ is the matrix exponential, $\boldsymbol{\eta}_i(t)$ is a three-dimensional independent standard-

Gaussian-random-number vector at a fixed time t with zero mean $\langle \boldsymbol{\eta}_i(t) \rangle = \mathbf{0}$ and diagonal deviation matrix $\langle \boldsymbol{\eta}_i(t)\boldsymbol{\eta}_i^T(t) \rangle = \mathbf{1}$ for updating the momentum vector of the *i*-th atom, and each element of the 3×3 matrix $\boldsymbol{\eta}^{(g)}(t)$ is defined as an independent standard-Gaussian-random-number at a fixed time t with zero mean $\langle \eta_{\alpha\beta}^{(g)}(t) \rangle = 0$ and $\langle \eta_{\alpha\beta}^{(g)}(t)\eta_{\alpha'\beta'}^{(g)}(t) \rangle = \delta_{\alpha\alpha'}\delta_{\beta\beta'}$.

■ AUTHOR INFORMATION

Corresponding Author

*E-mail: jianliupku@pku.edu.cn

ORCID

Jian Liu: 0000-0002-2906-5858

Notes

The authors declare no competing financial interests.

■ ACKNOWLEDGMENT

We thank Xiangsong Cheng for helpful discussions. This work was supported by the National Science Fund for Distinguished Young Scholars Grant No. 22225304 and by the National Natural Science Foundation of China (NSFC) Grant No. 22450002. We acknowledge the High-performance Computing Platform of Peking University, Beijing Beilong Super Cloud Computing Co., Ltd., Beijing PARATERA Tech Co., Ltd., the Beijing Super Cloud Computing Center (BSCC), the Computility Network of CAS, IKKEM Intelligent Computing Center and Guangzhou supercomputer center for providing computational resources.

■ **References:**

(1) Herman, M. F.; Bruskin, E. J.; Berne, B. J., On Path Integral Monte Carlo Simulations. *The Journal of Chemical Physics* **1982**, *76*, 5150-5155. http://dx.doi.org/10.1063/1.442815
(2) Martyna, G. J.; Hughes, A.; Tuckerman, M. E., Molecular Dynamics Algorithms for Path Integrals at Constant Pressure. *The Journal of Chemical Physics* **1999**, *110*, 3275-3290. http://dx.doi.org/10.1063/1.478193
(3) Tuckerman, M. E.; Berne, B. J.; Martyna, G. J.; Klein, M. L., Efficient Molecular Dynamics and Hybrid Monte Carlo Algorithms for Path Integrals. *The Journal of Chemical Physics* **1993**, *99*, 2796-2808. http://dx.doi.org/10.1063/1.465188
(4) Liu, J.; Li, D.; Liu, X., A Simple and Accurate Algorithm for Path Integral Molecular Dynamics with the Langevin Thermostat. *The Journal of Chemical Physics* **2016**, *145*, 024103. http://dx.doi.org/10.1063/1.4954990
(5) Shiga, M.; Shinoda, W., Calculation of Heat Capacities of Light and Heavy Water by Path-Integral Molecular Dynamics. *The Journal of Chemical Physics* **2005**, *123*. http://dx.doi.org/10.1063/1.2035078
(6) Tuckerman, M. E.; Liu, Y.; Ciccotti, G.; Martyna, G. J., Non-Hamiltonian Molecular Dynamics: Generalizing Hamiltonian Phase Space Principles to Non-Hamiltonian Systems. *The Journal of Chemical Physics* **2001**, *115*, 1678-1702. http://dx.doi.org/10.1063/1.1378321
(7) Martyna, G. J.; Tuckerman, M. E.; Tobias, D. J.; Klein, M. L., Explicit Reversible Integrators for Extended Systems Dynamics. *Molecular Physics* **1996**, *87*, 1117-1157. http://dx.doi.org/10.1080/00268979600100761
(8) Zhang, Z.; Yan, K.; Liu, X.; Liu, J., A Leap-Frog Algorithm-Based Efficient Unified Thermostat Scheme for Molecular Dynamics. *Chinese Science Bulletin* **2018**, *63*, 3467-3483. http://dx.doi.org/10.1360/N972018-00908
(9) Zhang, Z.; Liu, X.; Chen, Z.; Zheng, H.; Yan, K.; Liu, J., A Unified Thermostat Scheme for Efficient Configurational Sampling for Classical/Quantum Canonical Ensembles Via Molecular Dynamics. *The Journal of Chemical Physics* **2017**, *147*, 034109. http://dx.doi.org/10.1063/1.4991621
(10) Li, D.; Chen, Z.; Zhang, Z.; Liu, J., Understanding Molecular Dynamics with Stochastic Processes Via Real or Virtual Dynamics. *Chinese Journal of Chemical Physics* **2017**, *30*, 735-760. http://dx.doi.org/10.1063/1674-0068/30/cjcp1711223
(11) Li, D.; Han, X.; Chai, Y.; Wang, C.; Zhang, Z.; Chen, Z.; Liu, J.; Shao, J., Stationary State Distribution and Efficiency Analysis of the Langevin Equation Via Real or Virtual Dynamics. *The Journal of Chemical Physics* **2017**, *147*, 184104. http://dx.doi.org/10.1063/1.4996204
(12) Gao, X.; Fang, J.; Wang, H., Sampling the Isothermal-Isobaric Ensemble by Langevin Dynamics. *The Journal of Chemical Physics* **2016**, *144*, 124113. http://dx.doi.org/10.1063/1.4944909
(13) Zhang, Z.; Liu, X.; Yan, K.; Tuckerman, M. E.; Liu, J., Unified Efficient Thermostat Scheme for the Canonical Ensemble with Holonomic or Isokinetic Constraints Via Molecular

Dynamics. *The Journal of Physical Chemistry A* **2019**, *123*, 6056-6079. http://dx.doi.org/10.1021/acs.jpca.9b02771
(14) Smith, W.; Forester, T., Dl_Poly_2. 0: A General-Purpose Parallel Molecular Dynamics Simulation Package. *Journal of Molecular Graphics* **1996**, *14*, 136-141. http://dx.doi.org/10.1016/S0263-7855(96)00043-4
(15) Tuckerman, M. E.; Alejandre, J.; López-Rendón, R.; Jochim, A. L.; Martyna, G. J., A Liouville-Operator Derived Measure-Preserving Integrator for Molecular Dynamics Simulations in the Isothermal–Isobaric Ensemble. *Journal of Physics A: Mathematical and General* **2006**, *39*, 5629-5651. http://dx.doi.org/10.1088/0305-4470/39/19/S18
(16) Tuckerman, M. E., *Statistical Mechanics: Theory and Molecular Simulation*. Oxford University Press: Oxford ; New York, 2010.
(17) Lippert, R. A.; Predescu, C.; Ierardi, D. J.; Mackenzie, K. M.; Eastwood, M. P.; Dror, R. O.; Shaw, D. E., Accurate and Efficient Integration for Molecular Dynamics Simulations at Constant Temperature and Pressure. *The Journal of Chemical Physics* **2013**, *139*, 164106. http://dx.doi.org/10.1063/1.4825247
(18) Di Pierro, M.; Elber, R.; Leimkuhler, B., A Stochastic Algorithm for the Isobaric–Isothermal Ensemble with Ewald Summations for All Long Range Forces. *The Journal of Chemical Theory and Computation* **2015**, *11*, 5624-5637. http://dx.doi.org/10.1021/acs.jctc.5b00648
(19) Berendsen, H. J. C.; Postma, J. P. M.; Van Gunsteren, W. F.; DiNola, A.; Haak, J. R., Molecular Dynamics with Coupling to an External Bath. *The Journal of Chemical Physics* **1984**, *81*, 3684-3690. http://dx.doi.org/10.1063/1.448118
(20) Rogge, S. M. J.; Vanduyfhuys, L.; Ghysels, A.; Waroquier, M.; Verstraelen, T.; Maurin, G.; Van Speybroeck, V., A Comparison of Barostats for the Mechanical Characterization of Metal–Organic Frameworks. *The Journal of Chemical Theory and Computation* **2015**, *11*, 5583-5597. http://dx.doi.org/10.1021/acs.jctc.5b00748
(21) Bernetti, M.; Bussi, G., Pressure Control Using Stochastic Cell Rescaling. *The Journal of Chemical Physics* **2020**, *153*, 114107. http://dx.doi.org/10.1063/5.0020514
(22) Andersen, H. C., Molecular Dynamics Simulations at Constant Pressure and/or Temperature. *The Journal of Chemical Physics* **1980**, *72*, 2384-2393. http://dx.doi.org/10.1063/1.439486
(23) Hottovy, S.; McDaniel, A.; Volpe, G.; Wehr, J., The Smoluchowski-Kramers Limit of Stochastic Differential Equations with Arbitrary State-Dependent Friction. *Communications in Mathematical Physics* **2015**, *336*, 1259-1283. http://dx.doi.org/10.1007/s00220-014-2233-4
(24) Case, D. A.; Aktulga, H. M.; Belfon, K.; Cerutti, D. S.; Cisneros, G. A.; Cruzeiro, V. W. D.; Forouzesh, N.; Giese, T.; Goetz, A. W.; Gohlke, H., et al., Ambertools. *Journal of Chemical Information and Modeling* **2023**, *63*, 6183-6191. http://dx.doi.org/10.1021/acs.jcim.3c01153
(25) Case, D. A.; Aktulga, H. M.; Belfon, K.; Ben-Shalom, I. Y.; Berryman, J. T.; Brozell, S. R.; Cerutti, D. S.; Cheatham III, T. E.; Cisneros, G. A.; Cruzeiro, V. W. D., et al., *Amber 2023*. University of California, San Francisco: 2023.
(26) Kalibaeva, G.; Ferrario, M.; Ciccotti, G., Constant Pressure-Constant Temperature Molecular Dynamics: A Correct Constrained *Npt* Ensemble Using the Molecular Virial. *Molecular*

Physics **2003**, *101*, 765-778. http://dx.doi.org/10.1080/0026897021000044025
(27) Hünenberger, P. H., Calculation of the Group-Based Pressure in Molecular Simulations. I. A General Formulation Including Ewald and Particle-Particle–Particle-Mesh Electrostatics. *The Journal of Chemical Physics* **2002**, *116*, 6880-6897. http://dx.doi.org/10.1063/1.1463057
(28) Marry, V.; Ciccotti, G., Trotter Derived Algorithms for Molecular Dynamics with Constraints: Velocity Verlet Revisited. *The Journal of Computational Physics* **2007**, *222*, 428-440. http://dx.doi.org/10.1016/j.jcp.2006.07.033
(29) Ryckaert, J.-P.; Ciccotti, G.; Berendsen, H. J., Numerical Integration of the Cartesian Equations of Motion of a System with Constraints: Molecular Dynamics of N-Alkanes. *The Journal of Computational Physics* **1977**, *23*, 327-341. http://dx.doi.org/10.1016/0021-9991(77)90098-5
(30) Andersen, H. C., Rattle: A "Velocity" Version of the Shake Algorithm for Molecular Dynamics Calculations. *Journal of Computational Physics* **1983**, *52*, 24-34. http://dx.doi.org/10.1016/0021-9991(83)90014-1
(31) Miyamoto, S.; Kollman, P. A., Settle: An Analytical Version of the Shake and Rattle Algorithm for Rigid Water Models. *Journal of Computational Chemistry* **1992**, *13*, 952-962. http://dx.doi.org/10.1002/jcc.540130805
(32) Kräutler, V.; Van Gunsteren, W. F.; Hünenberger, P. H., A Fast Shake Algorithm to Solve Distance Constraint Equations for Small Molecules in Molecular Dynamics Simulations. *Journal of computational chemistry* **2001**, *22*, 501-508.
(33) Melchionna, S.; Ciccotti, G.; Lee Holian, B., Hoover Npt Dynamics for Systems Varying in Shape and Size. *Molecular Physics* **1993**, *78*, 533-544. http://dx.doi.org/10.1080/00268979300100371
(34) Shinoda, W.; Shiga, M.; Mikami, M., Rapid Estimation of Elastic Constants by Molecular Dynamics Simulation under Constant Stress. *Physical Review B* **2004**, *69*, 134103. http://dx.doi.org/10.1103/PhysRevB.69.134103
(35) Quigley, D.; Probert, M. I. J., Langevin Dynamics in Constant Pressure Extended Systems. *The Journal of Chemical Physics* **2004**, *120*, 11432-11441. http://dx.doi.org/10.1063/1.1755657
(36) Martyna, G. J.; Tobias, D. J.; Klein, M. L., Constant Pressure Molecular Dynamics Algorithms. *The Journal of Chemical Physics* **1994**, *101*, 4177-4189. http://dx.doi.org/10.1063/1.467468